REPORT DOCUMENTATION PAGE

Form Approved
OMB No. 0704-0188

1. AGENCY USE ONLY (Leave blank)	2. REPORT DATE	3. REPORT TYPE AND DATES COVERED
	April 1990	Final 22 Jan 90 - 21 Jun 91

4. TITLE AND SUBTITLE

Second ARO Workshop on Rotorcraft Interactional Aerodynamics

5. FUNDING NUMBERS

DAAL03-90-G-0037

6. AUTHOR(S)

N. M. Komerath

7. PERFORMING ORGANIZATION NAME(S) AND ADDRESS(ES)

Georgia Institute of Technology
Atlanta, GA 30332

8. PERFORMING ORGANIZATION REPORT NUMBER

9. SPONSORING/MONITORING AGENCY NAME(S) AND ADDRESS(ES)

U. S. Army Research Office
P. O. Box 12211
Research Triangle Park, NC 27709-2211

10. SPONSORING/MONITORING AGENCY REPORT NUMBER

ARO 27619.1-EG-CF

11. SUPPLEMENTARY NOTES

The view, opinions and/or findings contained in this report are those of the author(s) and should not be construed as an official Department of the Army position, policy, or decision, unless so designated by other documentation.

12a. DISTRIBUTION/AVAILABILITY STATEMENT

Approved for public release; distribution unlimited.

12b. DISTRIBUTION CODE

13. ABSTRACT (Maximum 200 words)

The workshop was held as scheduled. A report containing abstracts of the proceedings has been distributed by Georgia Institute of Technology.

14. SUBJECT TERMS

Rotocrafts, Rotorcraft Aerodynamics, Interactional Aerodynamics, Aerodynamics, Workshop, Rotors

15. NUMBER OF PAGES

16. PRICE CODE

17. SECURITY CLASSIFICATION OF REPORT	18. SECURITY CLASSIFICATION OF THIS PAGE	19. SECURITY CLASSIFICATION OF ABSTRACT	20. LIMITATION OF ABSTRACT
UNCLASSIFIED	UNCLASSIFIED	UNCLASSIFIED	UL

NSN 7540-01-280-5500

Standard Form 298 (Rev 2-89)
Prescribed by ANSI Std 239-18
298-102

27619.1-EG-CF

SECOND A.R.O. WORKSHOP ON ROTORCRAFT INTERACTIONAL AERODYNAMICS

ABSTRACTS OF PROCEEDINGS

SPONSORED BY:
U.S. ARMY RESEARCH OFFICE
RESEARCH TRIANGLE PARK, N.C.

THE SCHOOL OF AEROSPACE ENGINEERING
GEORGIA INSTITUTE OF TECHNOLOGY
ATLANTA, GEORGIA 30332

MARCH 26 - 27, 1990

GIT/AER-90-1

THE VIEWS, OPINIONS, AND/OR FINDINGS CONTAINED IN THIS REPORT ARE THOSE OF THE AUTHOR AND SHOULD NOT BE CONSTRUED AS AN OFFICIAL DEPARTMENT OF THE ARMY POSITION, POLICY, OR DECISION, UNLESS SO DESIGNATED BY OTHER DOCUMENTATION.

PROGRAM

Monday, March 26, 1990

8:45 a.m. Welcome: W. D. Freeston, Associate Dean of Engineering, Georgia Institute of Technology

9:00 a.m. "Fundamental Research Issues Underlying Helicopter Interactional Aerodynamics". T.L. Doligalski, Army Research Office

9:30 a.m. "Interactional Aerodynamics: A Review of Current Applications and Research Requirements". L. Dadone, Boeing Helicopters, Inc.

10:00 a.m. Break

10:15 a.m. "Full-Scale Investigation of Rotor/Fuselage Interaction". D.B. Signor, T.R. Norman, G.K.Yamauchi, NASA Ames Research Center

10:45 a.m. "Experimental Rotorcraft Flowfield Research at LARC/ASTD" D.R. Hoad, S.L. Althoff, J.W. Elliott, Army Aerostructures Directorate, Langley Research Center

11:15 a.m. "Computational Rotorcraft Research at LARC/ASTD" J.D.Berry, S.L. Althoff, Army Aerostructures Directorate, Langley Research Center

11:45 a.m. Lunch

1:30 p.m. "Comparison of Calculated and Measured Airloads on a Body-Rotor Combination". D.Clark and B.M. Maskew, Analytical Methods Inc.

2:00 p.m. "Propeller-Wing Interactions". R.Johnston, J.Sullivan, Purdue University

2:30 p.m. Break

2:45 p.m. "The Efficient Calculation of Rotor Flows Including Blade-Vortex Interactions Using Vortex Embedding". J.Steinhoff, Flow Analysis Inc. & U.Tennessee Space Institute, and K. Ramachandran, Flow Analysis, Inc.

3:15 p.m. "Studies of Rotor-Body Interactions in Forward Flight". N-P. Bi, G.L. Crouse, and J.G. Leishman, University of Maryland.

4:00 p.m. Discussion

5:00 p.m. Adjourn

Tuesday March 27

8:30 a.m. "New Vortex/Surface Interaction Methods for the Prediction of Wake-Induced Airframe Loads". T.R. Quackenbush, Continuum Dynamics, Inc, D.B. Bliss, Duke University, G. Lam, Continuum Dynamics, Inc., and A. Katz, Duke University.

9:00 a.m. "The Interaction of a Rotor Wake and an Airframe With and Without Flow Separation". J-M. Kim, O.A. Schreiber, S.G.Liou, N.M. Komerath, H.M.McMahon, Georgia Institute of Technology.

9:30 a.m. "Interaction of Discrete Vortices in Shear Flows Using High-Order Computational Schemes". R. Balasubramanian, Spectrex, Inc.

10:00 a.m. Break

10:15 a.m. "The Unsteady Interaction of a 3-Dimensional Vortex Filament with a Cylinder". H. Affes and A.T. Conlisk, Ohio State University

10:45 a.m. Discussion

12 noon Lunch

1:30 pm Tour of Georgia Tech School of Aerospace Engineering Rotorcraft Facilities.

INTERACTIONAL AERODYNAMICS: A REVIEW OF CURRENT APPLICATIONS AND RESEARCH REQUIREMENTS

L. Dadone

Boeing Helicopters
Philadelphia, Pa.

Second A.R.O. Workshop on Rotorcraft
Interactional Aerodynamics

Georgia Institute of Technology
Atlanta, Georgia

March 26-27, 1990

ABSTRACT: In rotorcraft aerodynamics, "interactional" effects are generally understood to be effects involving rotors and aircraft components. The subject is then subdivided into rotor-on-fuselage, fuselage-on-rotor, and rotor-on-rotor effects. From the point of view of analysis, interactional aerodynamic effects are difficult to model as they involve rotor wakes, fuselage/wing flow fields, and regions of separated flow. Rotors and fuselages are generally developed as "isolated" elements, and then combined with the help of experimental evidence.

Rotorcraft is a general term. In fact we are dealing with helicopters and with tilt-rotor aircraft, leaving aside, at this time, tilt-wing and other V/STOL concepts. In the helicopter arena many interactional problems have been identified and resolved long before analysis could really help. On the positive side, today, we are in a better position to address complex configurations in which mutual interference cannot be reduced by known approaches. Also, recent tilt rotor aircraft development efforts have benefitted from analytical and experimental research carried out over the past decade. But, in both helicopters and tilt rotor aircraft the toughest interactional problems remain to be properly understood and modeled.

This presentation will summarize the interactional aerodynamics research carried out at Boeing Helicopters since the mid-1970's. It will also address, from a manufacturer's point of view, the potential role of advanced computational methods in reducing the dependence on tests, while providing an additional insight which may lead to novel solutions.

Full-Scale Investigation of Rotor/Fuselage Aerodynamic Interactions

D.B. Signor, T.R. Norman, G.K. Yamauchi
NASA Ames Research Center

The Rotorcraft Aeromechanics Branch at NASA Ames is involved in a longstanding Interactional Aerodynamics program designed to quantify the aerodynamic and acoustic interactions between a main rotor, fuselage, and tail rotor. This paper will briefly review this program and provide more detailed information on the full-scale rotor/fuselage interaction test currently being conducted in the NASA Ames 40- by 80- foot wind tunnel.

Interactional Aerodynamics Program

The Rotorcraft Aeromechanics Branch's interactional aerodynamics program consists of three main elements: 1) full-scale testing, 2) small-scale testing, and 3) computational studies.

The first element of the program includes a series of full-scale main rotor and tail rotor tests. The first test of this element was with a Lynx tail rotor in forward flight conducted by the Royal Aircraft Establishment in their 24-ft wind tunnel (reference 1). Next, a hover test of a Lynx tail rotor was conducted at the NASA Ames Outdoor Aerodynamic Research Facility (reference 2). The primary objectives of these two tests were to acquire baseline performance and acoustic data for use in the subsequent 40- by 80- foot wind tunnel test with a main rotor. A secondary objective of the hover test was to investigate the effect of atmospheric turbulence on tail rotor acoustics. The third test of this element is the Bell Helicopter 412 main rotor and fuselage test which is currently in progress in the 40- by 80- foot wind tunnel (see below). The fourth and fifth tests will also be conducted in the 40- by 80- foot wind tunnel and are the planned Lynx tail rotor test and the planned full scale main rotor/fuselage/tail rotor test, respectively.

The second element of the program includes several small-scale tests. Two of these tests were conducted in the NASA Ames 7- by 10- foot wind tunnel and are documented in references 3 and 4. A third test, sponsored by this Branch, was conducted at Bell Helicopter (reference 5). These tests, utilizing a rotor and body of revolution mounted on separate balances, studied the effect of varying certain parameters (rotor/fuselage spacing, thrust, angle of attack, etc.) on aerodynamic loads. Some of the data acquired during these tests will

be used for comparison with the current full-scale rotor/fuselage interaction test.

The third element of the program includes correlation of test data with CFD and CAMRAD/JA predictions.

Full-Scale Rotor/Fuselage Interaction Test

The objectives of the current rotor/fuselage interaction test include the following: 1) improve the understanding of aerodynamic interactions between a main rotor and fuselage, 2) provide data for validation of wind tunnel wall correction methods, and 3) provide blade acceleration data for individual blade control (IBC) studies.

The primary measurements of this test include fuselage body pressures, fuselage loads, rotor loads, acoustics, and wall pressures. Details are included in table 1. The rotor loads are obtained by subtracting the fuselage loads from the wind tunnel balance loads.

The test model consists of a Bell 412 main rotor mounted on a Bell 576 test module, shown in figure 1. The axisymmetric body has a planform of a 30.74% - thick NACA four-digit symmetric airfoil forward of 66.5% of the body length and a straight line to the tail cone. The maximum diameter is 6.63 feet and the body length is 22.75 feet. The fairing has 111 static and 11 dynamic pressure taps, and is mounted on three independent load cells.

The Bell 412 is a soft in-plane, tapered tip, four-bladed rotor with a 23 foot radius, solidity of 0.064, and a nominal RPM of 324.

The test configurations include: body with hub, body with hub and rotor, and body alone. Details are included in table 2.

References

1. Owen, T. B. and Beauchamp, A. R.: Aero-Acoustic Measurements on a Lynx Tail Rotor in the RAE 24-Foot Wind Tunnel. RAE-TM-Aero-1972, July 1983.
2. Signor, D. B.; Yamauchi, G. K.; Smith, C. A.; and Hagen, M. J.: Performance and Loads Data from an Outdoor Hover Test of a Lynx Tail Rotor. NASA TM 101057, June 1989.
3. Smith, C.A. and Betzina, M. D.: Aerodynamic Loads Induced by a Rotor on a Body of Revolution. Journal of the American Helicopter Society, 31, (1), January 1986.
4. Betzina, M. D.; Smith, C. A.; and Shinoda, P: Rotor/Body Aerodynamic Interactions. NASA TM 85844, October 1983.
5. Trept, T: A 0.15 Scale Study of Configuration Effects on the Aerodynamic Interaction Between Main Rotor and Fuselage. NASA CR 166577, January 1984.

Table 1. Full-Scale Rotor/Fuselage Test Measurements

- COMBINED ROTOR/FUSELAGE
  - Model lift, drag, and pitching moment (measured with the wind tunnel balance system)
- FUSELAGE
  - Fuselage lift, drag, and pitching moment (measured with independent load cells)
  - Steady and unsteady surface pressures
- ROTOR
  - Blade moments (at six radial stations)
  - Flap angle, lead-lag angle, pitch angle, pitch link loads
  - Blade accelerations (four accelerometers per blade: two in flap direction, two in chordwise direction)
- ACOUSTICS
  - Eight microphones
- TEST SECTION WALL PRESSURES
  - 32 ceiling taps
  - 27 east wall taps, 27 west wall taps
- OTHER
  - Mast bending moments

Table 2. Full-Scale Rotor/Fuselage Test Configurations

- BODY + HUB
  - shaft angle = -4 to -12 deg
  - V = 20 to 140 kts
  - rotor RPM = 324
- BODY + HUB + ROTOR
  - advance ratio = 0.05 to 0.3
  - shaft angle = -4 to -12 deg
  - tip Mach number = 0.60 and 0.68
  - collective pitch = 2 to 10 deg (approx.)
- BODY
  - shaft angle = 0 to -12 deg.
  - V= 20 to 140 kts
- TUNNEL EMPTY
  - 10 to 140 kts

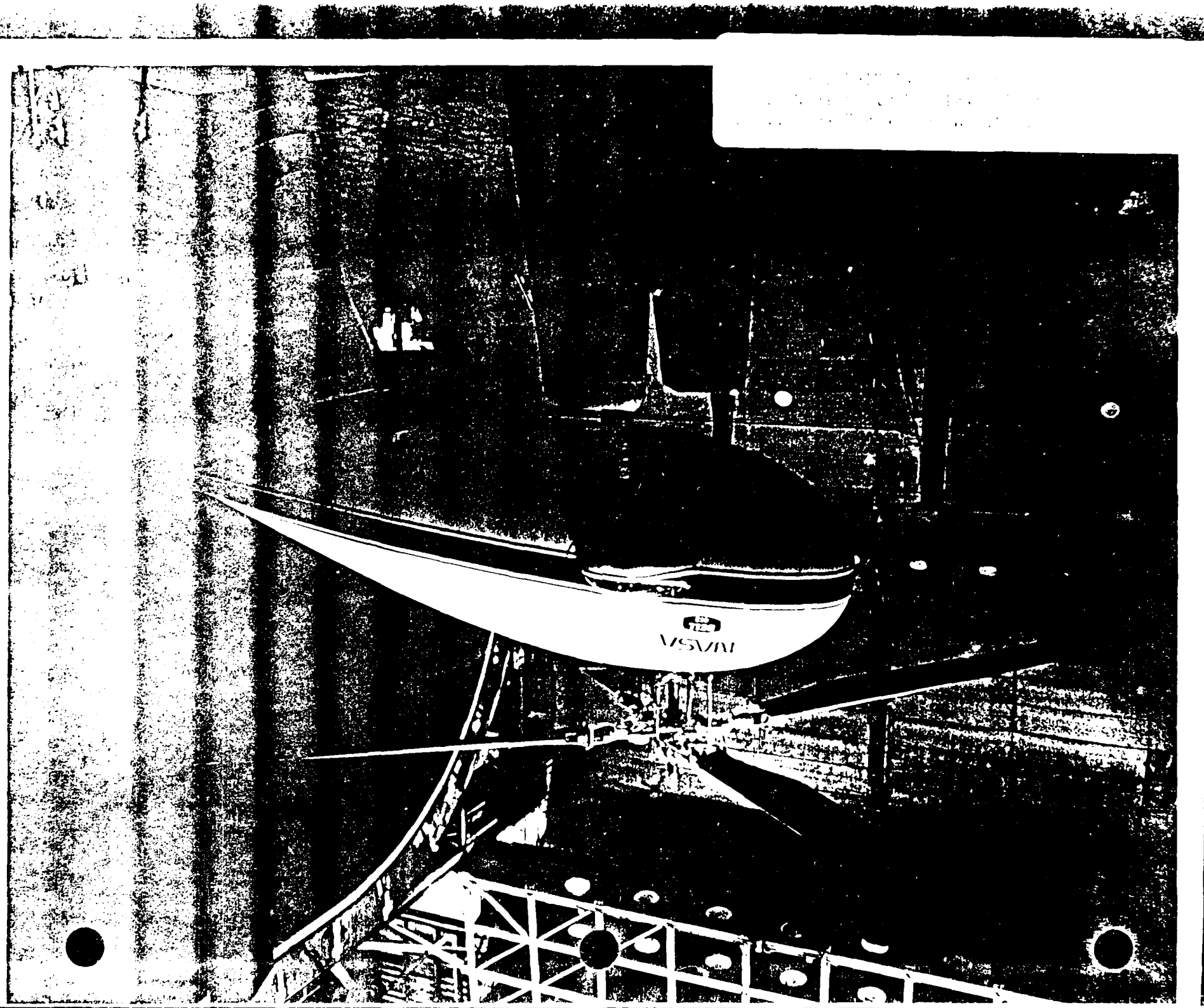

EXPERIMENTAL ROTORCRAFT FLOW FIELD RESEARCH AT LARC/ASTD

Danny R. Hoad, Susan L. Althoff, and Joe W. Elliott
NASA Langley Research Center
Mail Stop 286

Abstract of Presentation at
Second A.R.O. Workshop on Rotorcraft Interactional Aerodynamics
Georgia Institute of Technology
March 26-27, 1990
Atlanta, Georgia

Experimental helicopter wake and inflow research has been conducted in the 14- by 22-Foot Subsonic Tunnel at the NASA Langley Research Center for several years. In the past this effort, conducted by the Rotorcraft Aerodynamics Group (U.S. Army Aerostructures Directorate), has concentrated on the definition of the inflow characteristics to a generic rotor system using a laser velocimeter (LV). The resulting large data base includes a complete map of the temporal characteristics of the induced-inflow for several helicopter operating conditions - in two components - parallel to and perpendicular to the rotor tip-path-plane. The development of the inflow data base is intended to provide a comprehensive collection of high quality data for validation of existing and developing complex wake methods and to aid in the basic understanding of the general rotor flow field environment. Most recently, the experimental efforts have extended to rotor wake measurements and instantaneous measurement of the environment close to each of the rotor blades.

The inflow data base has now grown to include 11 sets of data for several rotor operating conditions. These include:

1. Two sets with tapered blades at a thrust coefficient of 0.0064, a propulsive force coefficient of 0, in a plane one-chord above the tip path plane:

   * Advance ratio = 0.15, and 0.23

2. Nine sets with rectangular blades at a thrust coefficient of 0.0064, and a propulsive force coefficient of 0:

   - at one-chord above the tip path plane:
     * Advance ratio = 0.15, 0.23, 0.30, 0.35, and 0.40

   - at 0.75-chord above the tip path plane:
     * Advance ratio = 0.23, and 0.30

   - at 0.50-chord above the tip path plane:
     * Advance ratio = 0.23, and 0.30

In all cases these inflow measurements were made at azimuthal increments of 30^0 from psi = 0 in a plane parallel to the

plane formed by the tips of the blades. Measurements were made from a radial location of r/R = 0.2 to r/R = 1.1, with the majority of the measurements concentrated toward the outboard portion of the disk. Analysis of the time-averaged results of these data has shown an unexpected large region of induced-upflow on the forward half of the rotor disk at high advance ratios. Correlations with existing wake methodologies have shown a discrepancy in this area. The effects of the fuselage presence have not been obvious in the data for advance ratios up to 0.30; however, above this value fuselage effects have been shown as an increased upflow along 180^0 azimuth. The temporal data in these data sets indicate that the largest four-per-rev oscillations in induced-inflow occur in the third quadrant of the rotor disc. Surprisingly the wake methods agree with the general area of maximum 4/rev oscillatory velocities, but not in magnitude. The data acquired in measurement planes closer than one-chord to the tip-path-plane (0.5- and 0.75-chord) are currently in analysis and preparation for publication.

In one of the recent inflow measurement programs, a carefully selected grid of measurement locations was chosen to provide data for the purpose of calculating the local blade bound circulation. Much like the efforts of John Ballard (1979) and Peter Lorber (1989), except at an advance ratio of 0.30, the measurements can be used to construct a circulation box about the lifting blade from which an integration of the local velocity vector in the direction of the box can compute the local circulation enclosed within the box. Recognizing that there are currently only two components of velocity available from this LV system, these measurements were made at an azimuth of 90^0 so that the desired measurements were orthogonal to the optical axis. Using CAMRAD predictions prior to the test program, a radial location was chosen which had the maximum circulation at 90^0 azimuth, and did not have any other form of circulation (tip vortices) entering the circulation box. These data are in analysis and preparation for publication. The objective for this process was to develop the measurement technique for use during one of the later Joint Army/Industry Inflow/Wake Research Programs in which local blade surface pressure measurements will be available. Correlation between blade circulation calculations using the laser velocimeter and the surface pressure measurements can provide confidence in the technique for future use.

The first test in the Joint Army/Industry Inflow/Wake Research Program was conducted in May of 1989 with Bell Helicopter Company. The program was conducted with the company model that incorporated 92 local blade surface pressures. The major objectives of the test program included reduced tip-speed inflow effects as well as rotor wake definition experiments, and correlation of these measurements with the blade surface measurements. The reduced tip-speed effects were examined at an advance ratio of 0.37, two thrust coefficients: 0.0064 and 0.0081, and two tip-speeds: 603 and 710 ft/sec. The rotor wake definition experiments included measurements at the four test conditions mentioned previously. At each of these conditions vapor screen flow visualization tests were conducted to define the wake geometry characteristics for correlation with wake methods and as a guide

for defining the particular locations of interest for laser velocimeter measurements. The second joint Army/Industry research program is currently scheduled for July 1990 with Boeing Helicopters. The test program is scheduled for a 4-week entry in the 14- by 22-Foot Subsonic Tunnel using the pressure-instrumented 360 rotor system tested in the DNW wind tunnel. Progress in the preparations for this program include manufacturing of the interface hardware to allow mating the Boeing rotor drive system to the wind tunnel model support equipment. The program will concentrate on measuring the characteristics of the vortex wake formation along the trailing edge of the advancing rotor blade primarily in the area where negative lift occurs at high advance ratio. Test plans also include blade circulation measurements with the laser velocimeter, and correlation with integrated rotor blade pressure data at various chord positions is of interest.

In the area of rotor/fuselage interaction, the Aerostructures Directorate (ASTD) is a participant in a Memorandum of Understanding (MOU) between the U.S. Department of Defense and the French Ministry of Defense. Comparisons of the prediction capability of rotor/fuselage interaction methods will be shared. Experimental data obtained in both France and the U.S. will be exchanged to establish a broad data base for code validation (? calibration ?). Currently, the schedule calls for an ASTD researcher's participation in a 10-week 3-component laser velocimeter wind tunnel test program at the ONERA S2 (Chalais-Meudon), and an ONERA researcher's participation in a 2-component laser velocimeter wind tunnel test at the 14- by 22-Foot Subsonic Wind Tunnel. The ONERA test program is scheduled for a mid-April wind tunnel entry. It will use a model of the Aerospatiale Dauphine, and will concentrate on defining the flow environment near the fenestron and emmpenage. Vapor screen flow visualization techniques with the laser will be used to define the rotor/fuselage flow field in lateral planes along the model. The operating conditions for this test are an advance ratio of 0.20 and 1-g flight simulation. The U.S. test program is planned for the fall 1990. It will use the Army's 2-Meter Rotor Test System with a generic rotor and fuselage, and the 14- by 22-Foot Subsonic Tunnel 2-component laser velocimeter. The research objectives will concentrate on definition of the rotor hub wake separation effects. Vapor screen flow visualization will also be used in this definition process.

Computational Rotorcraft Flowfield Research At the U.S. Army AeroStructures Directorate

John D. Berry and Susan L. Althoff
AeroStructures Directorate, U.S. Army Aviation Systems Command
NASA Langley Research Center, Hampton, Virginia

Background

Rotorcraft aerodynamic interaction investigations are conducted by the U.S. Army at the NASA Langley 14- by 22-Foot Subsonic Tunnel. These investigations are conducted using both experimental and computational methods. The aspects of experimental investigations have been described by Mr. Hoad in his presentation. To support an understanding of the complex nature of the flowfield of a rotorcraft several computational efforts have been pursued at the AeroStructures Directorate (ASTD.)

A method of predicting airloads on the rotorcraft fuselage using a steady vortex ring model for the rotor and wake was developed by Freeman in 1979. This method accounted for both the contraction of the wake and the static pressure rise within the wake stream tube. Pressure correlation with steady experimental measurements was good.

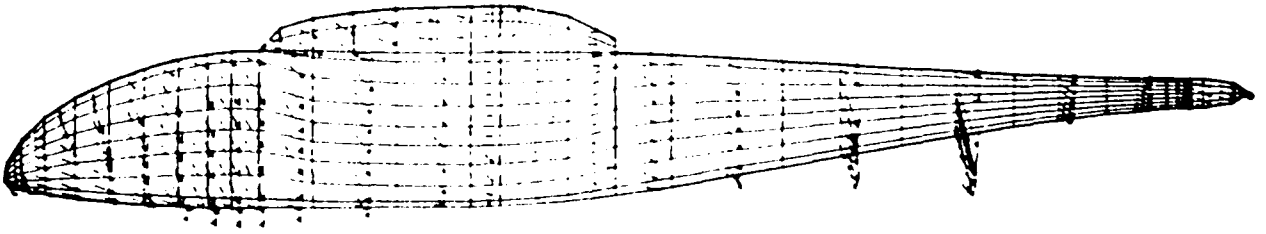

Figure 1. Fuselage Velocity Computation (Freeman)

A method of predicting unsteady loading on the fuselage due to a periodic rotor wake was developed at the United Technologies Research Center by Lorber and Egolf under contract to this directorate. The method uses the established generalized distorted wake method developed by Egolf and Landgrebe and a fuselage panelling method developed by Sheehy at Sikorsky Aircraft. This method invokes a localized wake distortion, prescribing a jump in filament location from above the body to beneath the body. An additional feature of this method is the inclusion of unsteady pressure terms derived from the unsteadiness of the potential associated with the moving blades and wake.

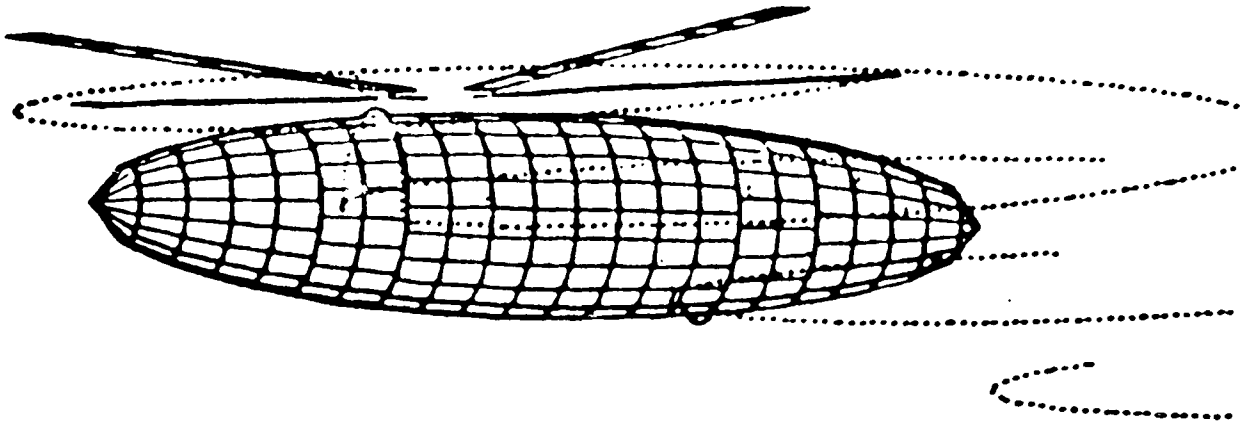

Figure 2. UTRC Interactional Aerodynamics Method

An in-house computational method has been developed as a general purpose tool for the analysis of general rotor/wake/fuselage configurations in unsteady motion. The rotor wake is convected with the local induced velocities from the rotor, other wake elements, and the fuselage. Loading on the rotor blades is computed using vortex panels responding the velocities of the freestream, the rotational velocity, and all elements of induced velocity. This vorticity associated with this loading is shed into the wake through time-marching. The resulting wake captures a time-accurate distribution of vorticity.

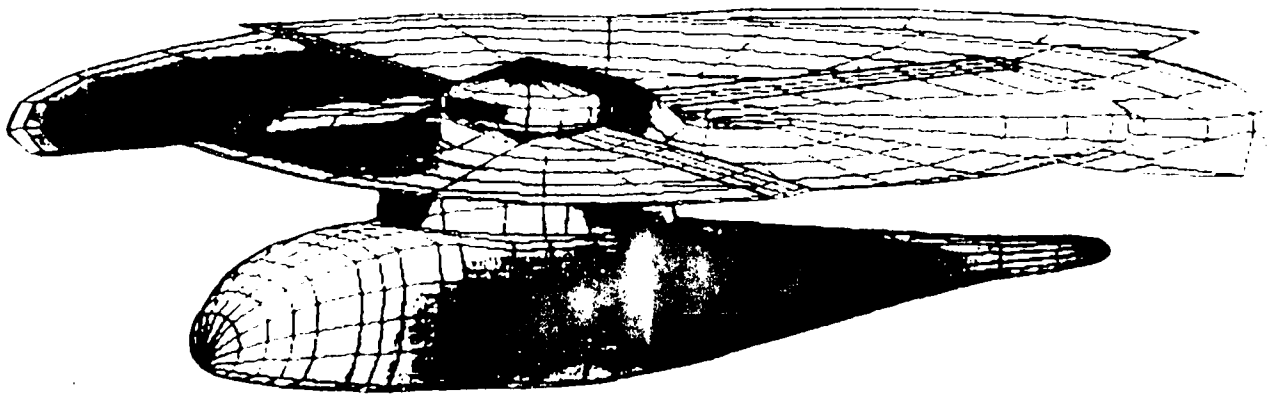

Figure 3. LaRC/ASTD Rotor/Wake/Fuselage Method

The in-house method of rotor/wake/fuselage (RWF) computation has been applied to two interactional problems. The first problem is the experiment conducted at Georgia Tech using a two bladed rotor to generate wake interaction on a cylindrical fuselage. For this problem the RWF method is used to predict the location of the tip filament core as it passes over the nose of the cylindrical fuselage. The second problem studied are the velocity measurements obtained with laser velocimetry above a lifting rotor/fuselage configuration at the Langley 14- by 22-Foot Subsonic Tunnel. In this problem RWF is used to assess the relative velocity perturbations in the inflow to the rotor due to the fuselage.

Georgia Tech Tip Trajectory Study

The specific configuration studied for the Georgia Tech experiment is a case where the rotor hub is located 0.3 radii above the fuselage center-line and 1.0 radii behind the nose of the fuselage. The ratio of forward speed to tip speed is 0.10 and the collective of the untwisted blades is fixed at 10 degrees. The general configuration used for the calculations is shown below (hub spacing is increased for clarity.)

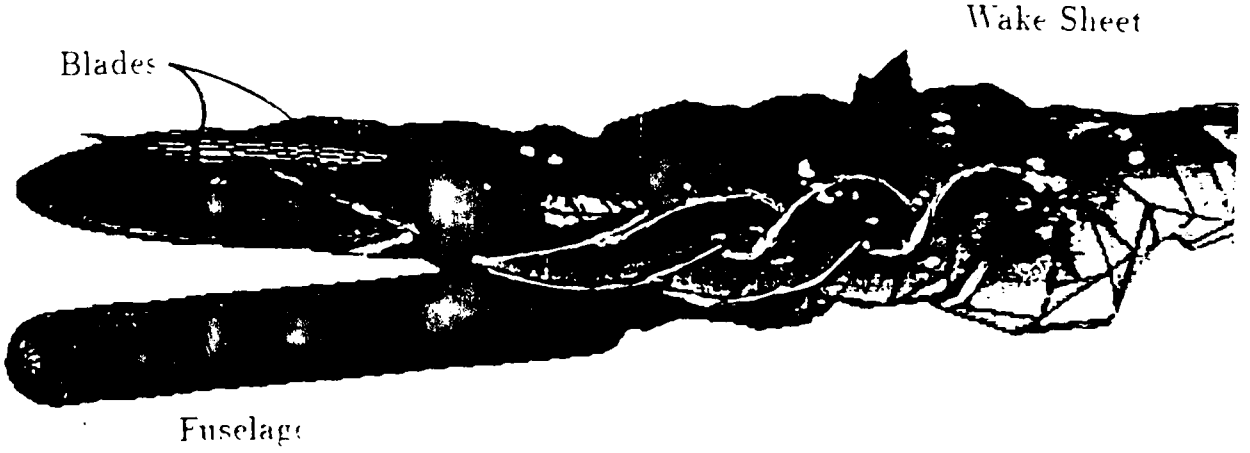

Figure 4. Predicted Wake Geometry

The tip vortex is defined by straight line segments between control points for the wake. Convection of the wake is computed by displacing the control points by the product of the local instantaneous velocity and the delta time (azimuth) step. In the figure below the resulting distorted tip vortex trajectory is shown (again, hub spacing increased for clarity.) In this figure the vortex filament segment closest to the fuselage is seen to stretch apart at the fuselage center-line as well as to slow in downstream velocity. This stretching causes one filament, connecting the two points separating over the center-line, to closely approach the surface.

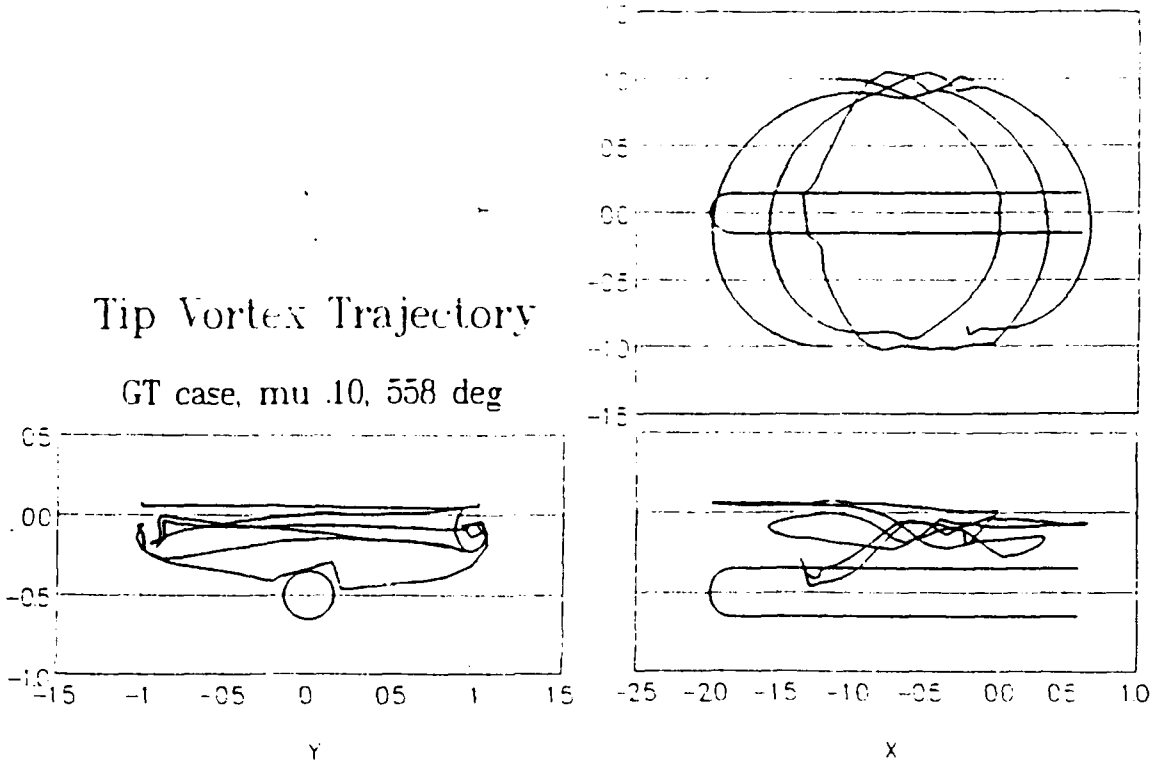

Figure 5. Three-view of Tip Vortex Trajectory

The calculations of tip vortex trajectory are made by averaging the location of the two outer-most filaments. The next figure shows the correlation between experimentally observed tip vortex trajectory and the computed trajectory. The experimental observations are purely periodic, whereas the computations are the result of time-marching a solution from an impulsive wake initiation. Thirteen vortex locations are shown from the experiment. The six-degree time steps for teh computations are shown for each of the two wake sheets. The computational trajectory is computed by determining the intersection of the filament with the centerplane of the fuselage. Locations of the control points are not shown in the following figure. Although the computed trajectory is shown to pass into the fuselage, the control points are observed to remain outside the fuselage boundary. The darkened square symbols indicate the time at which the wake sees the passage of the second blade overhead.

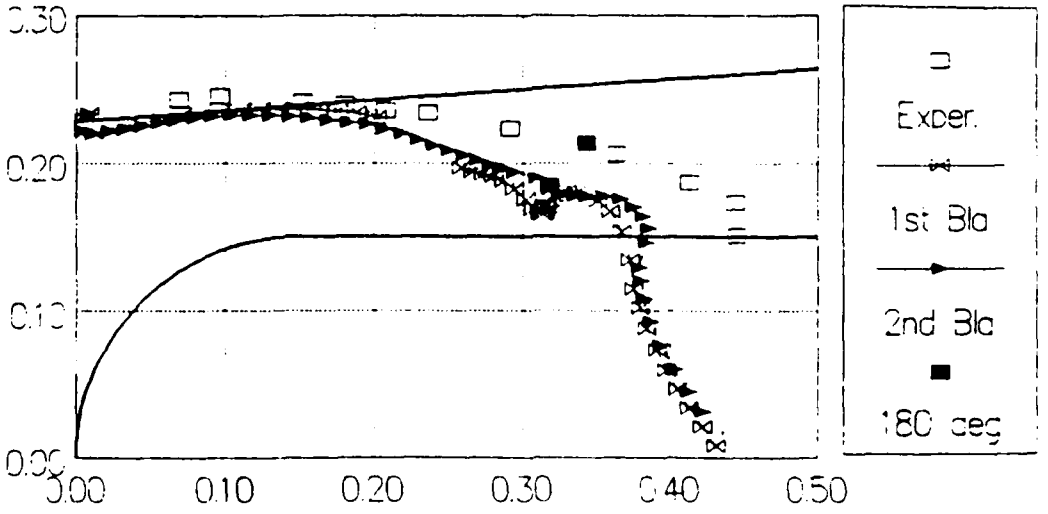

Figure 6. Side View of Tip Vortex Trajectory

Two significant differences between the experimentally observed trajectory and the computed trajectory are seen: First, the initial vertical location of the tip vortex is not computed well. This results in a larger upward displacement of the wake sheet and a farther downstream impact with the fuselage. The second difference is the non-linear displacement near the time of second blade passage and passage of the filament within the fuselage. The difference between the first wake tip trajectory and second wake tip trajectory indicate that although the initial displacement is identical, the fuselage impact location is moving farther aft.

The trajectory of the tip vortex is represented well by the computed geometry. However, details of two aspects of the problem need further investigation. The actual formation of the edge of the vortex sheet, also known as the tip vortex, is not accurately captured using the inviscid vortex lattice technique used here. The second aspect of the problem is the viscous interaction between the vortex sheet and the surface boundary layer. Filament stretching is not captured with sufficient fidelity in the technique demonstrated here.

The Langley Inflow Velocity Study

The effects of a fuselage on the loading of the rotor has been of interest for a long time. Several methods have been used to assess and quantify these effects. The influence of the fuselage will primarily be seen as a perturbation to the onset flow to the rotor. From a "strip theory" point of view the effect of this perturbation will cause a change in effective blade element angle of attack.

An experimental program to assess the flow velocity field at the rotor disk has been conducted at the LaRC 14- by 22-Foot Subsonic Tunnel by the Army's Rotorcraft Aerodynamics Group. This inflow program has been producing maps of the inflow velocity field to a characteristic rotor operating at characteristic conditions above a characteristic fuselage. These inflow maps, therefore, contain the perturbations from the experimental fuselage configuration. The figure below is an example of the inflow velocity ratio map obtained at an advance ratio of 0.23.

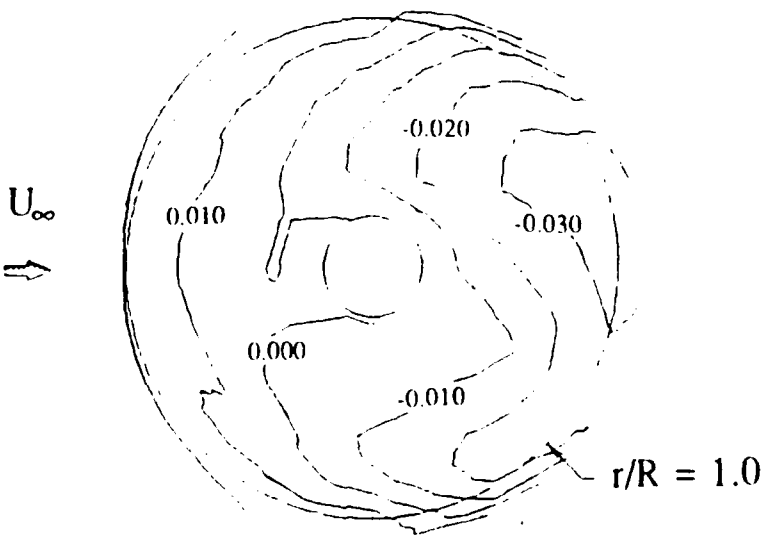

Figure 7. Inflow Ratio at 0.23 Advance Ratio.

To assess the magnitude of the fuselage perturbations two techniques have been used. The first technique uses a panel representation of the fuselage to obtain the velocity field at the location where the experimental velocities are measured. The panel method uses simple source panels with only the freestream velocity as a boundary condition. The second technique uses the fully interactive RWF method described above to compute the full perturbation field at the experimental measurement locations. By using the RWF method to compute the perturbation velocity field both with and without the fuselage in the computations, a difference in the two velocity fields will be the effect of the fuselage.

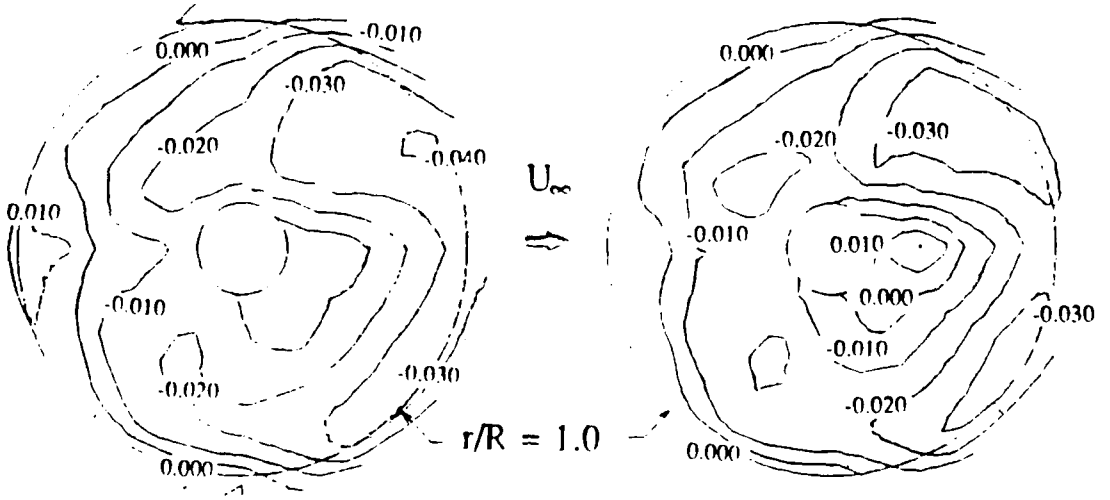

(a) With Fuselage Model (b) Without Fuselage Model

Figure 8. Predicted Inflow Ratio

The difference between the velocity perturbation computed by differencing the RWF results with and without a fuselage and the perturbations derived from the fuselage in freestream model gives the effect of wake perturbations and the effect of rotor and wake induced flow on fuselage singularity distributions. The following figure shows this difference at one advance ratio for the specific configuration studied.

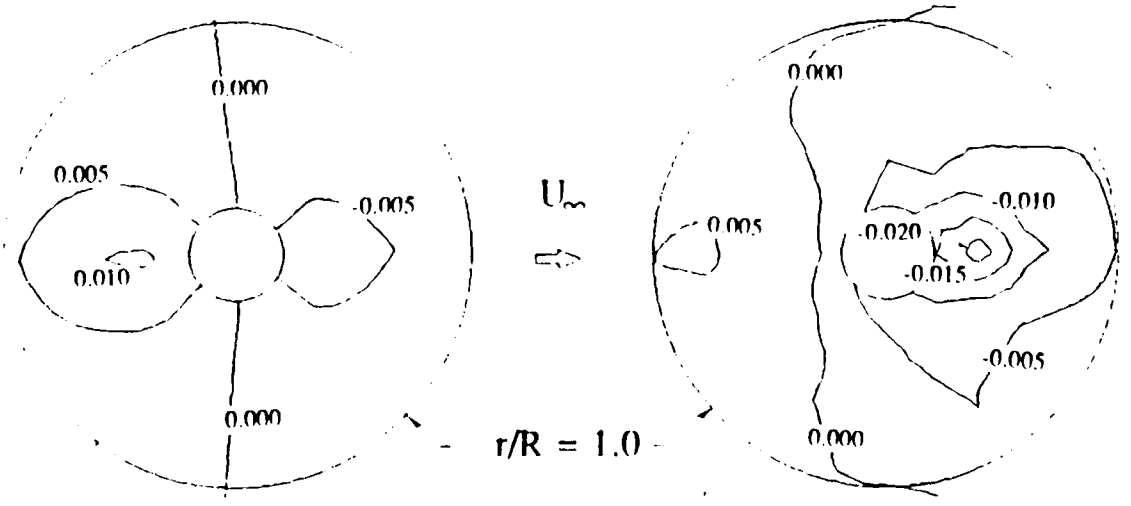

(a) Perturbations due to Isolated Fuselage (b) Perturbations due to RWF Fuselage

Figure 9. Comparison of Isolated Fuselage and RWF Velocity Perturbations.

Conclusions

Calculations can predic' the periodic geometry of a rotor wake. Details of the wake interactions with the fuselage surface are not well modeled with inviscid panel methods. Fully unsteady calculations of the effects oi a rotor wake on the fuselage of a rotorcraft configurations must be made to assess the complete set of interactional effects. For the cases studied here the overall effects of the fuselage are relatively small. However, increasing the size of the fuselage or decreasing the fuselage-rotor spacing will amplify these effects.

ABSTRACT

"Comparison of Calculated and Measured Airloads on a Body/Rotor Combination"

by

David R. Clark and Brian Maskew
Analytical Methods, Inc.
Redmond, Washington

Second ARO Workshop on Rotorcraft Interactional Aerodynamics

March 26 - 27, 1990

Georgia Institute of Technology
Atlanta, Georgia

ABSTRACT

The paper will present the status of a study under way at Analytical Methods, Inc. exploring the application of a second generation, low-order panel method operating in the time domain to helicopter configuration modeling problems. Based on the widely used VSAERO (for Vortex Separation AEROdynamics) program the new method, program USAERO (for UnSteady AEROdynamics), employs the same combination of doublet and source singularities for body modeling and doublet singularities for wake modeling. Beyond this, the unsteady effects are incorporated by operating in the temporal domain using a time-stepping technique and establishing at each step the time rate of change of the doublet distribution.

Using this technique it is possible to model most dynamic events. In the present study, where modeling of a full vehicle in dynamic flight is a program goal, the effort has been concentrated on developing a correlation base by gradually increasing the scale and complexity of the configurations modeled. For this presentation, three of these early configurations will be explored. They are an isolated 4-bladed rotor (H-34) operating at $\mu = 0.3$; a simple 2-bladed teetering rotor with a close coupled cylindrical fuselage (the Georgia Institute of Technology Model); and a more involved, 4-bladed rotor/body combination (the University of Maryland Model).

Results from all three cases will be presented. In the H-34 case the results will be used to demonstrate the method's ability to predict rotor system dynamic loads and in the two other cases rotor on body effects will be explored.

This work was funded in part by an SBIR contract administered by the Army Research Office.

Flow Visualization of Propeller Tip Vortex Interaction

Robert T. Johnston
John P. Sullivan
Purdue Aerospace Sciences Laboratory

In order to understand the nature of the propeller wake interaction with lifting surfaces, a series of flow visualization studies have been co..ducted at Purdue University. The motion of a helical tip vortex over a wing, over a stator, and through the second stage of a counter rotational propeller have been considered to date.

Studies have been done on steady state propeller/wing aerodynamic interactions. Steady state measurements revealed that a lift enhancement, and wing drag reduction is possible with certain geometries of a tractor configuration propeller. Flow visualization studies were initiated to understand the unsteady nature of the propeller/wing interaction. The geometry of the propeller/wing vortex interaction is in some respects similar to that of a helicopter main rotor vortex being cut by the tail rotor during flight.

The propeller/wing interaction study revealed that as the propeller tip vortex moves toward the wing leading edge it progressively deforms until the viscous effects in the vicinity of the leading edge cause the vortex filament to pinch off with the segments ending on the upper and lower wing surfaces. This severed vortex filament moves along the airfoil and reconnects at the trailing edge.

Wing angle of attack was successively set to ± 5 and 10 degrees. At both of these angles noticeable changes were apparent in the motion of the tip vortex. First, there is a chordwise misalignment in the tip vortex as the vortex moves along the airfoil. Under conditions of propeller absorbing power the spanwise shear is outward on the upper surface on the upwash side. With the propeller in a loaded condition the vortex shears outward below the wing on the propeller upwash side. On the propeller downwash side there is no noticeable spanwise shear under powered propeller conditions, while the propeller absorbing power condition exhibits only slight outward movement of the vortex core on the upper surface. Wing angle of attack was set to -5°, for the power absorbing propeller case, and the spanwise shearing rotated 180° as expected.

Investigation into the propeller/stator vortex interaction was first modelled by mounting a stationary propeller blade behind a rotating propeller. The propeller operated at both power absorption and power output conditions, creating a change in rotation (sign) of the propeller tip vortex. For the case of positive stator angle of attack and power absorbed by the propeller, a prominent winding effect was observed. A strong vortex interaction also occurs for the powered propeller condition and a negative angle of attack on the stator. The other two cases lead to a stator vortex breakdown and little structured vortex interaction.

The third phase of the flow visualization experiment involved running two identical straight bladed propellers in a two-by-two counter rotation arrangement. The counter rotation propeller study revealed that the second stage imparts a distortion in the tip vortex of the first stage. The vortex/vortex interaction contributes to early helical vortex breakdown, as compared to the case of a single propeller helix.

Propeller-wing and propeller/propeller aerodynamic interaction, when fully understood, could lead to improvements in propulsion efficiency. Design of aircraft will have to address the propeller slipstream effects on the wings in order to fully exploit the favorable aspects of the interaction; reduced drag, and lift enhancement. Design of CRP systems may benefit from knowledge of the flow field through reduction in noise and vibration. Numerous studies have been performed to date, yet this interaction is still not fully understood.

The authors would like to acknowledge the support of the NASA Lewis Research Center in this ongoing research.

The Efficient Calculation of Rotor Flows Including Blade-Vortex Interactions Using Vortex Embedding

John Steinhoff
University of Tennessee Space Institute & Flow Analysis, Inc. Tullahoma, TN

K. Ramachandran
Flow Analysis, Inc. Moffett Field, CA

Abstract

The accurate computation of rotor flows requires the proper treatment of strong, concentrated vortex sheets that are produced by rotor blades and convect near other blades. For modern rotors, it also requires the proper treatment of compressibility effects, including shocks, which can occur near the blades. Different methods have existed for some time for efficiently treating each of these separately, but not simultaneously.

Euler or Navier–Stokes equation solution methods using surface fitted, fixed grids have been shown to give accurate results for compressible flows, even in the presence of shocks. However, when concentrated vortices are present, these fixed grid, or Eulerian methods result in large amounts of unphysical numerical diffusion, unless high order schemes are used, together with a dense computational grid. These methods capture compression discontinuities or shocks well, in a few grid points, but not contact discontinuities, or vortex sheets. The internal structure of shocks is not resolved and solved for. Instead, special shock operators are used, which result in an ad-hoc shock structure. The details of this structure are not important since the thickness is small, and as long as conservation laws are obeyed, integrated through the discontinuity, good results are obtained for the flow field. Vortex sheets or contact discontinuities, however, are not treated in a similar way: Vorticity is assumed to be present everywhere in the field and the same finite difference equations used elsewhere are used to solve for the structure in vortex sheets. As a result of this lack of special treatment, sheets which may initially be concentrated over only a few grid cells tend to diffuse fairly rapidly when convected through the flow.

Potential Flow methods also use fixed, Eulerian grids, are fully compressible and can capture shocks. Contact discontinuities, or vortex sheets, however, are treated as potential discontinuities and do not diffuse. They are typically fixed on grid planes and do not follow the flow. Compressible Potential Flow solutions conserve mass throughout the field as do Euler/Navier–Stokes methods. They also conserve momentum everywhere that there are no vortex sheets. Because contact discontinuities are constrained to lie on grid surfaces, however, Potential Flow solutions typically do not conserve momentum through vortex sheets.

Because of the diffusion or constraint problems associated with the treatment of vortex sheets, the above methods, by themselves, do not appear to be the most efficient way of treating rotor problems, where these sheets must be accurately computed.

Methods which seem to be more appropriate for treating concentrated vortex sheets include Vortex Lattice schemes. They use a Lagrangian method to compute the sheets by representing them by sets of markers which follow the flow. Typically, an integral expression is then used to compute velocity by integrating over the markers. No numerical diffusion results since the internal structure of the vortex sheet is, effectively, determined by the integral representation near the markers rather than solved for with a finite differences scheme. Good results have been obtained with these methods for incompressible flows. These successes show that, for many rotor flows, a detailed computation of the internal structure of the vortex sheets is not important: The overall shape and strength of the sheets, which must follow the

local flow, are the important factors. (In some cases, the thickness of the sheet may also be relevant, since it can affect self-induced velocities.) It can be shown that these vortex sheet calculations, effectively, conserve momentum, integrated through the sheet. The formulae used to compute velocity by integrating over the sheets results in velocities which conserve mass. Besides not representing compressible flows, the basic vortex lattice methods have other drawbacks; For detailed calculations with large numbers of markers, or if velocity must be computed at many field points, the number of computations required increases rapidly. In addition, cases where the vortex sheet impinges on a blade and where the internal structure is important are typically outside the scope of these methods.

The limitations of each of the above individual methods for treating some aspect of the rotor problem have led people to use separate methods in different regions of the field and patch the solutions together: Separate computational boxes have been defined around each blade where Eulerian method are used, and Lagrangian Vortex Lattice methods used to treat the vortex sheets outside these boxes. Velocities computed from both methods are matched on the outer surfaces of the computational boxes. Unfortunately, accurate compressible solutions require that the outer boundary of these boxes be a number of chords away from the blade surfaces, while a number of vortex sheets can come closer than this to the blade. This makes a clear separation of the two aspects of the problem difficult.

The Vortex Embedding Method is a combined Eulerian/Lagrangian technique which attempts to overcome these difficulties. A single, blade fixed, unified grid is used which encompasses the entire rotor-disk region with all of the blades. On this grid, the mass balance relation is satisfied using a compressible, conservative finite volume formulation, as in Eulerian schemes. The vortex sheets which are shed from each blade, however, are defined by a set of markers which move with the flow, as in Lagrangian schemes. These markers move through the Eulerian grid and carry the vorticity. Accordingly, two coupled solution methods are used: The marker positions are computed based on total velocities interpolated from the Eulerian grid, and the mass balance equations are solved on the Eulerian grid with vorticity defined by interpolation from the markers.

A particularly simple way to do this involves the use of a velocity decomposition on the Eulerian grid:

$$\boldsymbol{q} = \boldsymbol{q}^{\omega} + \nabla\phi + \boldsymbol{\Omega} \times \boldsymbol{r}, \tag{1}$$

where $\boldsymbol{\Omega}$ is the rotor rotational vector. The $\boldsymbol{q}^{\omega}$ component, which defines the vorticity, is carried by the markers and interpolated from them. The interpolation formula, effectively, determines the vortex internal structure as defined on the Eulerian grid. Mass balance, based on total velocity, $\boldsymbol{q}$, is effected by computing a potential, ϕ at each grid point using an efficient, implicit approximate factorization method to solve the finite volume mass balance relation in each grid cell:

$$\partial_x(\rho u) + \partial_y(\rho v) + \partial_z(\rho w) = 0 \tag{2}$$

where ρ is the density and has the isentropic form away from the sheet based on the total velocity, $\boldsymbol{q}$, with components u, v and w.

$$\rho = \left\{ 1 - \left(\frac{\gamma - 1}{2} \right) M_\infty^2 ((\boldsymbol{\Omega} \times \boldsymbol{r})^2 - \boldsymbol{q}^2) \right\}^{\frac{1}{\gamma - 1}}$$

The vortical component, $\boldsymbol{q}^{\omega}$, is spread over several grid points around the vortex sheet so that vorticity is concentrated there.

During iteration towards convergence (the solution is steady in the blade coordinate system for hover), a four step procedure is repeatedly used:

1) The vortex sheet position is integrated as a set of marker streamlines to follow the flow using interpolated values of $\boldsymbol{q}$ from the fixed grid.
2) $\boldsymbol{q}^v$ is computed at grid points near the sheet.
3) A potential, ϕ, is computed at each grid point to satisfy eqn. (2), with $\boldsymbol{q}^v$ fixed.
4) A new velocity $\boldsymbol{q}$ is computed at each grid point based on eqn. (1).

At convergence eqn. (2) is satisfied and the vortex sheet follows the flow. A particularly simple and accurate form for $\boldsymbol{q}^v$ involves a Clebsch-type of representation:

$$\boldsymbol{q}^v = \Gamma^c \nabla \psi \tag{3}$$

where $\Gamma^c(\boldsymbol{r})$ is a three dimensional field which smoothly goes to the appropriate Γ (circulation value) on the sheet as $\boldsymbol{r}$ approaches the sheet surface. The potential, $\psi(\boldsymbol{r})$, smoothly goes from $+1/2$ on one side of the sheet to $-1/2$ on the other. A convenient formula for $\psi(\boldsymbol{r})$ is

$$\psi(\boldsymbol{r}) = \frac{1}{2}\, sin\,(\pi S_n), \quad |S_n| < a/2 \tag{4a}$$

$$\psi(\boldsymbol{r}) = +1/2, \qquad S_n > +a/2 \tag{4b}$$

$$\psi(\boldsymbol{r}) = -1/2, \qquad S_n < -a/2 \tag{4c}$$

where S_n is a (signed) normal distance from the point $\boldsymbol{r}$ to the sheet, and a is a specified spreading distance (several grid cells).

We use interpolation-like formulae to compute $\Gamma^c(\boldsymbol{r})$ and $S_n(\boldsymbol{r})$ at any grid point $\boldsymbol{r}$. Even though ψ is non-zero throughout the field (except on the sheet), $\nabla\psi$ is zero beyond the spreading distance from the sheet. Accordingly, both $\Gamma^c(\boldsymbol{r})$ and $\psi(\boldsymbol{r})$ need be computed only on those grid points that are in a narrow band about the sheet with thickness of the order of the spreading distance. Another very important property of this $\boldsymbol{q}^v$ is the elimination of spurious numerical vorticity in regions near the sheet where Γ is constant (no physical vorticity on the sheet). In such regions, $\Gamma^c(\boldsymbol{r})$ will be constant and $\boldsymbol{q}^v$ can be written as

$$\boldsymbol{q}^v = \nabla\left[\Gamma^c \psi(\boldsymbol{r})\right] \tag{5}$$

Even though $\boldsymbol{q}^v$ is still non-zero, if the same numerical differencing scheme is used for $\nabla\psi$ as is used for $\nabla\phi$, the effect of the sheet in regions of zero vorticity will be identically zero.

It is important to realize that only short-range $\boldsymbol{q}^v$'s, such as given above, can be efficient for use in our scheme. If we had a long-range form, given, for example, by the Biot-Savart law, then the $\boldsymbol{q}^v$ calculation would have to be made for each point in the entire grid. Each of these calculations would effectively involve a 2-D integration over the entire vortex sheet. This part of the calculation would then be prohibitively expensive.

This method was first implemented in a code, **HELIX I**, which solves for rotor flows in hover. In addition to the Vortex Embedding method, an integral boundary layer scheme is implemented in **HELIX I**.

Results

Results of **HELIX I** computations and comparisons with experiments show the ability of the code to predict the wake structure, high speed loading, profile drag and finally the entire lift/power curve.

Rotor data containing both loading and wake information are available for a two bladed, rectangular, untwisted rotor of low aspect ratio and a NACA0012 profile. Figure 1 shows a comparison of the computed and measured axial and radial convection of the tip vortex. The initial axial convection rate, K_1, is very well predicted. The subsequent axial rate, K_2,

is initially underpredicted. This is due to a large spreading parameter used for this case, which was required in our earlier versions of the code (before our use of Clebsch variables). Subsequent calculation do not have this problem. However, K_1 is the most important of the two parameters because it determines the vortex distance of closest approach to the blade. The radial contraction is initially overpredicted also due to our (modeled) spreading, however, it rapidly converges to the experimental value for $\psi = 180^o$ and all subsequent azimuths. Thus the free wake prediction correctly gives the relative position of the first vortex passage with respect to the blade. Figure 2 shows the resulting predicted and measured loading in the form of chordwise pressure distributions. This case is highly transonic ($M_T = 0.877$) and it is seen that the measured shocks are well predicted. The point here is that a free wake and transonic solution can be handled by a unified analysis. This particular computation would require a surface grid refinement if an accurate drag computation were to be performed. Unfortunately power is not available for this data.

As a first step in demonstrating the ability to predict power, comparisons were made with experimental data for a nonlifting rotor with an untapered, untwisted rectangular planform and a NACA0012 profile. In addition to pressure drag we also included the integration of skin friction calculated from the boundary-layer model. Figure 3 is a plot of the measured power coefficient, C_Q, as a function of rotor tip Mach number together with **HELIX I** computations. The power variation is well predicted especially in the M_T range 0.6-0.8. The differences seen at lower speed can be due to the boundary layer being laminar and not well predicted by the present turbulent boundary layer model. the transonic drag divergence is fairly well predicted, with the computed rise being at a slightly higher tip Mach number than the data indicates. This level of accuracy is more than adequate for hover purposes, where induced power constitutes the major loss.

Finally, we require comparisons of predicted wakes and total power. We compare **HELIX I** results for a four-bladed rotor with -8^o linear twist and a rectangular planform with experimental data by Landgrebe for three different collective pitch angles, $\Theta_{.75}$ (pitch at $r/R = 0.75$). The axial and radial convection of the tip vortex for collective pitch angles of $6^o, 8^o$ and 10^o is shown in Figs. 4 and 5. For this rotor prediction of K_1 and K_2 are excellent. (The data symbols shown are obtained from Landgrebe empirical formulae.) In Fig. 5 the tip vortex radial contraction is plotted as a function of azimuth and good comparison is seen for the vortex location up to the first passage ($\psi = 90^o$) for the 8^o and 10^o cases. The computed vortex for the 6^o case is more inboard compared to the experimental data.

The computed performance power polar is shown in Fig. 6 and compared to experimental data. In this the torque coefficient is shown as a band that is bounded by values obtained from surface pressure integration and an energy flux integral. It is seen that the comparison of thrust/power for $\Theta_{.75} = 6^o$ and 8^o is excellent. At 10^o the power is somewhat overpredicted for presently unknown reasons. For these computations, the values used for pitch are the actual experimental values. Most other codes require a pitch correction (2^o is not uncommon) in order to match the experimental lift. Therefore a slight under-prediction of lift in these computations constitutes unusually good agreement - and probably results from the present wake modeling. This constitutes (to our knowledge) the first complete CFD (in the usual finite difference/finite volume sense) computation of rotor performance.

Extensions of the Vortex Embedding Method

The same Vortex Embedding method has been used to treat fixed, solid surfaces such as bodies and pylons, without requiring body-conforming grids. It has also been generalized so that blade-vortex impingement cases can be treated where the internal structure of the vortex is radically altered and must be computed. Preliminary results of these extensions will be presented.

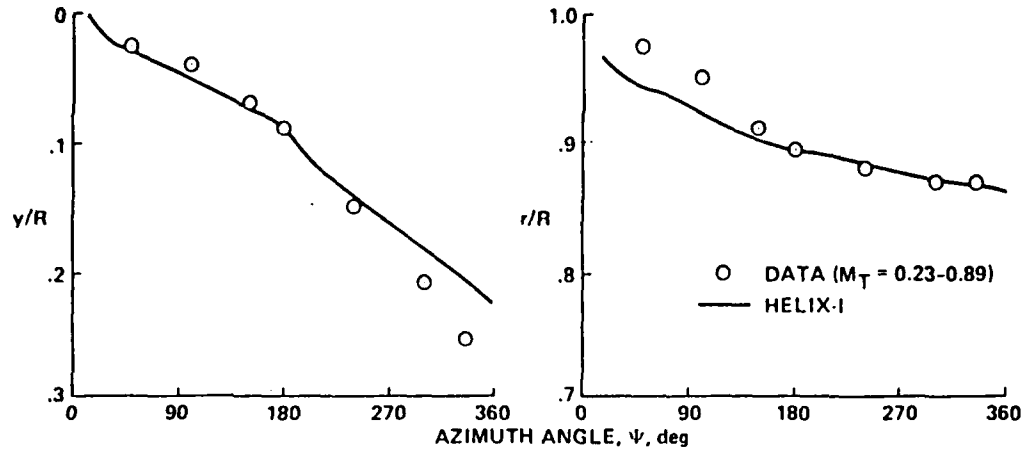

Fig. 1 Axial and radial convection of tip vortex. 2 bladed hovering rotor, rectangular, untwisted, NACA0012, Aspect Ratio = 6.0, $\Theta_{.75} = 8°$.

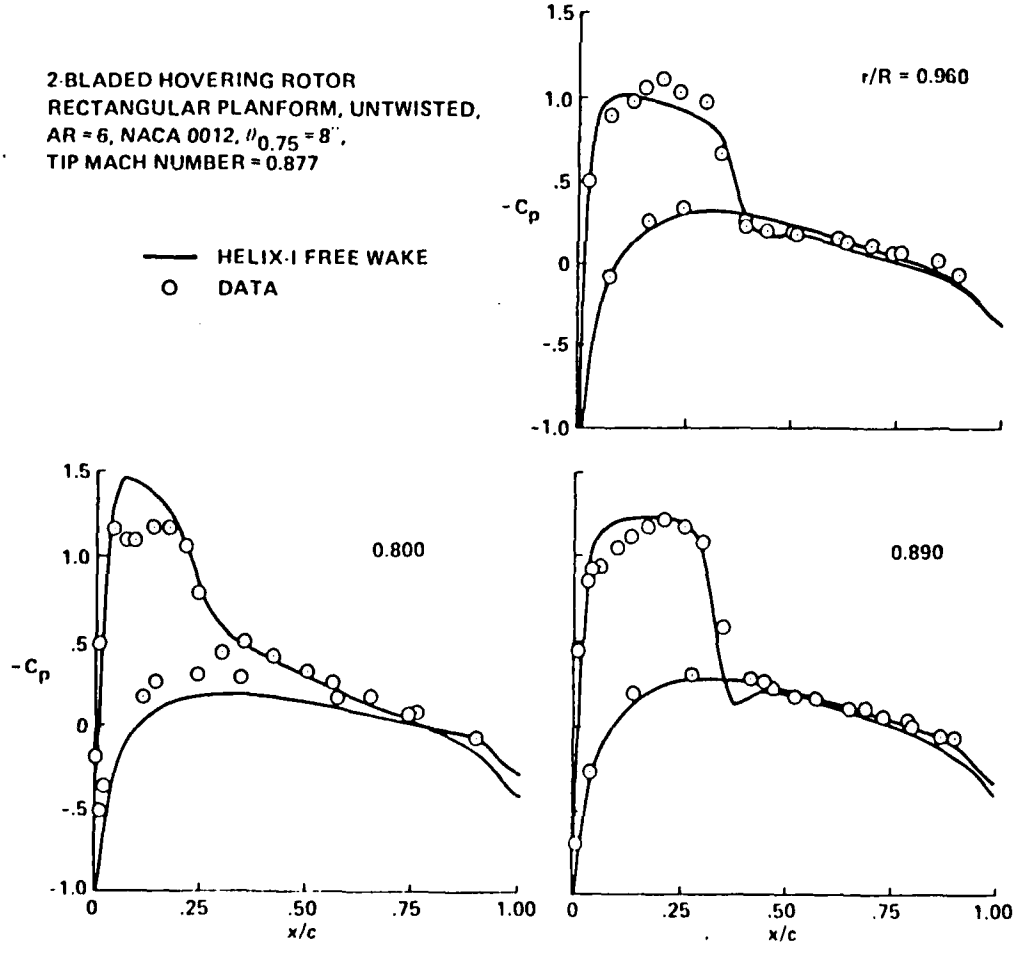

Fig. 2 Computed and measured loading on a rotor.

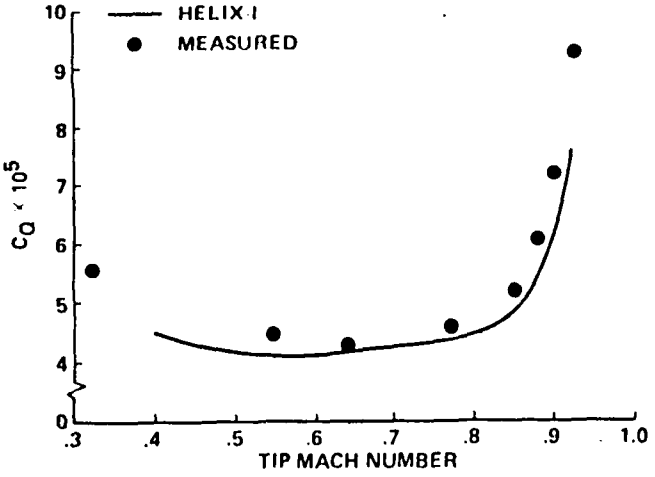

Fig. 3 Measured and computed hover profile power for a nearly nonlifting rotor. 2 blades, untapered, untwisted, NACA0012, Aspect Ratio = 13.7 $\Theta_{.75} = 0.75°$.

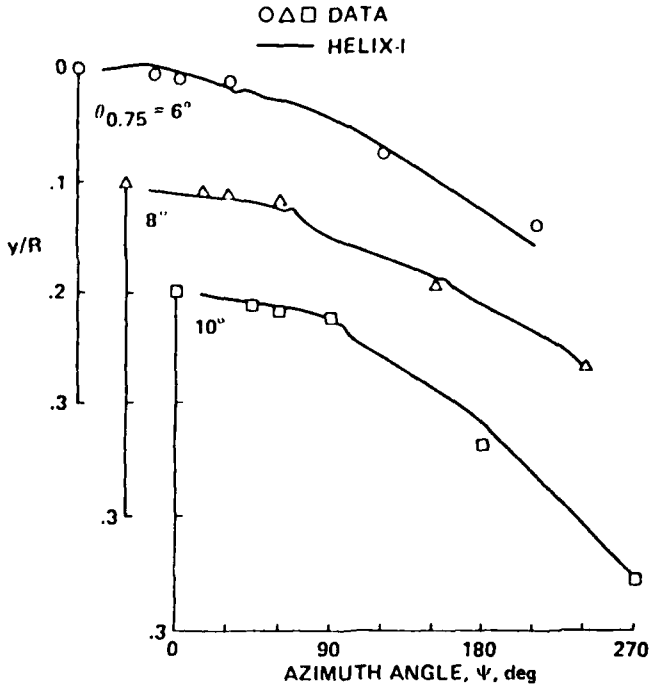

Fig. 4 Axial convection of tip vortex.

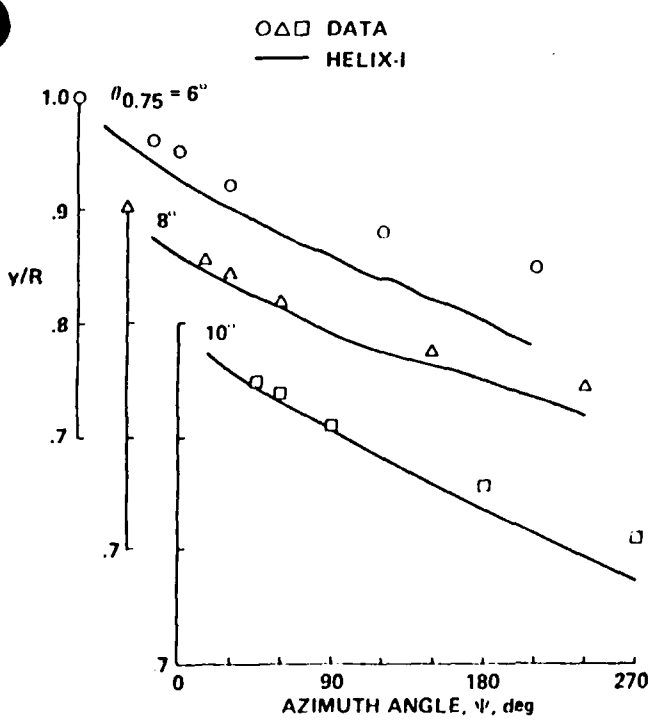

Fig. 5 Radial convection of tip vortex.

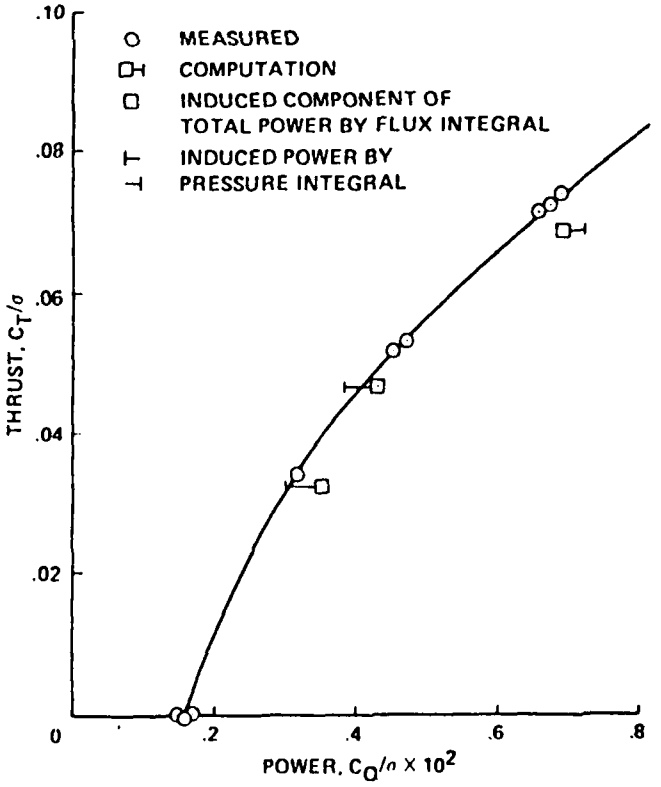

Fig. 6 Computed and measured rotor hover performance.

Studies of Rotor-Body Aerodynamic Interactions in Forward Flight

Naipei Bi
Research Assistant

G.L. Crouse
Graduate Fellow

J. G. Leishman
Assistant Professor

Center for Rotorcraft Education and Research
Department of Aerospace Engineering
University of Maryland,
College Park Maryland 20742

Summary

A series of experiments have been conducted to quantify both the time-averaged and the unsteady aerodynamic interactions between a rotor and a body in forward flight. These studies were complimented by a parallel theoretical analysis of the interaction problem. The objectives of this work were to provide an improved understanding of the interactional mechanisms occurring in a helicopter rotor/airframe environment, as well as to assess the capabilities and limitations potential flow/singularity methods in predicting these interactional effects.

1. Experimental Work

The experiments were performed in the Glenn L. Martin wind tunnel at the University of Maryland. This is a closed return tunnel with a 7 foot by 11 foot working section. The configuration tested was a 65 inch diameter four bladed rotor with a fully articulated hub. The rotor was driven by a 40HP hydraulic motor via a belt transmission. The rotor blades were of rectangular planform with a chord of 2.5 inches. These blades were constructed of graphite-epoxy and were structurally very stiff relative to a full scale rotor in order to minimize aeroelastic effects. The body consisted of an idealized, but representative, helicopter fuselage comprising a body of revolution with a 2.25:1 taper ratio.

1.1 Data Acquired

Primary data consisted of independent strain-gauge balance measurements for the rotor and fuselage loads, along with both steady and unsteady pressure loads at a number of points on the fuselage. Total rotor loads, such as thrust, were measured with a six component strain-gauge balance. A torque disk was used to measure the rotor power. A separate three component strain-gauge balance was used to measure lift, pitching moment and drag on the fuselage. Time-averaged pressures were measured at 142 points over the fuselage surface. These pressure taps were located in three rows along the top and sides of the fuselage and at two circumferential rings.

In addition, unsteady pressures were measured at 21 points on the fuselage. The sensors used were primarily concentrated over the nose and tail of the fuselage. The outputs from the transducers were connected to a CAMAC high speed data acquisition system which interfaced to an Hewlett-Packard HP1000/A400 minicomputer over an IEEE bus. Time histories of all the pressure transducer responses were logged over 10 rotor revolutions with a sampling resolution of 256 data frames per rotor revolution, i.e. an azimuth resolution of about 1.4 degrees. Triggering was enabled by a 1/rev and 256/rev TTL pulses synchronized with the rotor shaft. Further details on the rotor system and data acquisition procedures are given in Ref. 1

Other data measured data consisted of a comprehensive map time averaged flow field velocities. These data were obtained by traversing an array of 7-hole probes in planes below and behind the rotor. This information has provided significant quantitative information as to the locations of the rotor wake boundaries in forward flight, as well as the wake roll-up process. This work has also provided guidance for future studies with hot-wire and LV anemometry. Further details are given in Ref. 2.

Flow visualization data have also been obtained for the present rotor/fuselage configuration using smoke flow/laser sheet illumination, as well as wide-field shadowgraphy. The laser sheet visualization was moderately successful, however the shadowgraph studies have provided more detailed information on the location of discrete wake filaments in the flow. Some information has also been obtained on wake distortion due to the fuselage. These results are given in Ref. 3.

1.2 Test Conditions

Data were obtained for advance ratios, between 0.05 and 0.25, shaft tilt angles between -2 and -8 degrees, and collective pitch settings from 4 to 12 degrees. In all, some 200 separate test conditions have been examined to during the two wind-tunnel entries performed to date. The combined rotor/fuselage configuration was tested, as well as the isolated rotor and the isolated fuselage. The isolated cases were used to provide a baseline performance specification for comparative purposes.

1.3 Summary of Results

The results from the present experimental work have begun to clarify the mechanisms responsible for the complexity and the severity of the interactional aerodynamics effects between a rotor and fuselage combination. In general, the interactions were found to be highly unsteady at all points on the airframe. This reinforces the requirement that any theoretical analysis of the interactional problem must take unsteady effects into account. Specific findings from the present study are numerous, and are outlined below.

Significant redistributions of the time-averaged surface pressures were obtained on the fuselage surface, particularly in regions below the rotor and especially at the boundaries of the rotor wake. These pressure distributions were found to be very sensitive to changes in rotor thrust as well as advance ratio. With increasing thrust, the pressure peaks induced on the fuselage by the rotor wake increased significantly on the top and the sides of the fuselage. Increasing the advance ratio moved the pressure peaks further aft along the fuselage.

Because of these redistributions of surface pressure, fairly large changes in the total body forces and moments were obtained. A download and a nose-up pitching moment were obtained at low advance ratios; this download and moment generally increased with increasing rotor thrust, but decreased somewhat with increasing advance ratio. At higher advance ratios, an upload and a nose-down pitching moment were created. In addition, the induced pressures on the fuselage were found to be asymmetric with respect to the fuselage centerline, thereby producing as side force as well as a yawing moment.

In addition to the effects of the rotor on the fuselage loads, the fuselage itself was found to provide measurable changes in rotor performance. At low advance ratios, the presence of the fuselage was found to provide an increase in rotor thrust relative to the isolated rotor performance at a given collective pitch setting In some cases this increase was as much as 10% of the isolated rotor thrust. As the advance ratio was increased however, the effect of the fuselage on the rotor thrust was found to reduce such that at higher advance ratios (>0.15) there was little effect. In general, the increase in thrust on the rotor was found to be greater than the corresponding download on the fuselage. Interestingly, the presence of the fuselage was also found to reduce the rotor power required at a given thrust. Thus, it was surprizing that a net gain in total system performance was obtained with the fuselage present. Additional details are given in Ref. 1.

The unsteady pressure measurements on the fuselage were found to one of the most interesting parts of the experimental work. In most cases the magnitude of these unsteady pressure fluctuations were very large and clearly exceeded the time-averaged pressure values. However, the unsteady pressure fluctuations were not

necessarily the greatest in the regions of the highest time-averaged pressure. A vast amount of unsteady pressure data has been obtained, from which it has been possible to more fully identify and characterize the flow phenomena actually contributing to the interaction problem. One important finding is that it has been possible to separate out the effects of blade passage interactions from the effects due to wake interaction.

Three main types unsteady pressure signatures have been identified on the fuselage. The first type of signal was a result of blade passage. This was seen as a 4/rev. pulse and was the most dominant in locations directly under the rotor. The magnitude of the type of signal increased in proportion to the blade loading, but was almost totally independent of the advance ratio. Blade passage effects dropped off dramatically in regions away from the rotor.

The second type of unsteady pressure signature has been classified as a close wake-fuselage interaction. This occurred when a wake filament passed in close proximity to the fuselage, but did not necessarily strike the surface. This interaction produced a very characteristic "sawtooth" pressure signature as the wake vortex passed over a point on the fuselage. The magnitude of this type of signature depended mainly upon the proximity between the wake filament and the fuselage surface.

The third interaction was a result of direct wake impingement on the fuselage surface. This was the most complex type of interaction. Wake impingement was also characterized by a "sawtooth" type of wave form, but with several second peaks and many higher harmonics. The source of these secondary peaks is currently under more detailed study, but appears to be a result of the rotor vortex sheet structure. Further details are given in Ref. 4.

2. Theoretical Work

The theoretical analysis pursued in the present work mainly concerned the modeling of the unsteady effects associated with the rotor/body interaction problem. In the work, a more coherent attempt is made to identify and address the full significance of the various elements of the flowfield which contribute to the unsteady pressures on the fuselage. The procedure adopted was to first start with a simple and computationally efficient model of the problem, then whilst retaining all the relevant terms, to gradually increase the sophistication to a level which would permit the greatest flexibility for design purposes. The work draws on much of the experimental data discussed previously. The main objective of the work was to determine the limitations of potential flow/singularity methods in predicting the unsteady airloads on the fuselage, as well as to develop computationally efficient strategies to account for the more complex interactions. Details of the approach are given in Ref. 5.

Since the flow velocities in the vicinity of the fuselage are much smaller than the speed of sound, incompressible flow assumptions provided a useful simplification to the analysis. In steady incompressible flow, the pressure at any point is simply a function of the local velocity of the flow and the free stream conditions. However, in an unsteady flow the pressure at any point in the flowfield, say for example on the fuselage, must be obtained from Kelvin's equation. In general, by far the largest contribution to the the fuselage pressures are from the unsteady term in Kelvin's equation.

There are several phenomena in the flow field which can contribute to the unsteady term; such phenomena include a moving element in the flow (e.g. a moving wake filament or the moving bound vorticity on the blades) or a change in the strength of an element (e.g. the change in circulation about the blades with changing azimuth angle). However, the most dominant effect in the rotor/body interaction problem is the moving vortices in the flow.

2.1 Simplified Model

It is possible to make an exact analytical computation of the effects of the unsteady terms by using a simplified model of the rotor system and its wake. This type of approach has been found to provide considerable insight into the significance of the rotor and its wake on the unsteady fuselage airloads. One such simple model consists of representing the rotor by lifting lines of finite length, but with constant circulation along their span. The constant circulation assumption is quite reasonable for moderately/highly twisted rotors, as used in the present experimental study. The rotor wake was approximated by a series of vortex rings which are spatially located based on momentum theory considerations. The induced velocity from the vortex rings can be computed exactly in terms of elliptic integrals. The surface representing the fuselage is made a streamline to the flow by introducing an image system of lifting lines and vortex rings.

Use of this simple model has been shown to give very reliable estimates of the unsteady fuselage pressures. For example, both blade passage pressure signatures and wake vortex interaction pressure signatures have been predicted to a very acceptable level of accuracy when compared with the experimental measurements. In addition, it has possible to conduct very economical parametric studies to assess the effects of wake position on the unsteady surface pressures.

2.2 Higher Level Model

The higher level of modeling used in the present study was divided into four basic parts: (1) a source panel model of the fuselage, (2) a lifting line model for the rotor, (3) a prescribed wake model of the rotor wake, and (4) a simplified model of the interaction between the fuselage and the wake.

The fuselage was modeled using a classical 3-D source panel model developed in-house expressly for this analysis. The model was formulated using the basic Hess and Smith methodology, but was modified to include unsteady potential terms when calculating the fuselage surface pressures.

The rotor was modelled as a four lifting lines. In this study, the circulation distribution was determined at 10 points along each blade. For each azimuth angle, the inflow was calculated at these 40 points using a trailing wake algorithm. Each rotor blade induces a velocity field which can be calculated at any point in space by application of the Biot-Savart law. Unsteady effects on the rotor blades themselves are not taken into account in the present level of analysis since the the main effort is to compute the effects on the fuselage loads due to the rotor and its wake.

It was decided to eliminate the wake geometry as an unknown by using a prescribed wake model in which the geometry was derived from wake flow surveys as well as flow visualization. The rotor wake geometry was constructed by allowing the vortex filaments trailed from the rotor blade tips to roll up immediately into a single tip vortex situated at 95% radius. The strength of the tip vortex was assumed to be invariant with time, and was assigned a value based on the average of the peak bound circulation on the rotor. This provides a considerable simplification to the analysis. This assumption is realistic only at low advance ratios, however it is adequate for the present work which is confined to advance ratios of 0.15 or below. The wake filaments are then assumed to convect downstream at the local free-stream velocity. The vertical displacements of the wake were computed using a combination of momentum theory and empirically derived distortion factors derived from the experimental measurements.

The wake vortex filaments were discretized into straight line segments. At each time step the local velocity was calculated at the end points of the segments, followed by the calculation of the vortex position at the next time step. The local velocities at the required points in the flowfield were calculated using the Biot-Savart law. The unsteady contributions to the fuselage pressures due to the unsteady terms from the convecting wake filaments were calculated using a backward difference approximation.

The normal solution procedure is to first invert the fuselage influence matrix, which is invariant with time. The unknown array of source strengths at any time step are subsequently obtained by a simple matrix multiplication process using the updated values of the onset flow velocities. The unsteady velocity potential due to the changing source strengths were obtained using a backward difference approximation.

It should be noted, that the contribution to the time dependent terms due to the variation in source strength on the fuselage panels is usually neglected because its evaluation can be fairly time consuming. However, the results of the present study have shown that the

unsteady source strength contributions are significant, and must be retained in order to predict the unsteady pressures on the fuselage.

A simple, but novel, correction to the wake geometry due to the presence of the fuselage was also included in the analysis. While, the quasi-steady induced velocity from the wake is felt at all points on the fuselage, it is unnecessary to perform this calculation if only the unsteady loads are required. This provides a considerable reduction in computation effort. Nevertheless, it is still required to take into account the relative distortion of the wake as it comes in close proximity to the fuselage. The wake induced velocity on the fuselage is resolved into components normal and tangential to the surface. An additional unsteady source is then introduced at the center line of the fuselage, with a strength which exactly cancels the normal velocity at the surface of the body. The new velocity field is then calculated including the effects of this source. The tangential velocity is also corrected by using an approximate image vortex. The surface is locally assumed to be planar and an image vortex is placed to negate the normal velocity induced at the surface by the wake vortex. These two corrections allow the wake to drape itself over the surface in a very realistic manner (as observed in the experimental work) but whilst retaining computational efficiency.

While calculating the geometry of the wake, the length of individual vortex segments is also calculated. Since the wake passes over the surface, the segments are stretched quite significantly and so produces significant changes in strength of the vortices. In addition, the vortex viscous core size decreases as the vortex is stretched These effects are included, albeit approximately, in the calculation of the induced velocities during either a close interaction or a direct impingement of the wake vortices on the fuselage.

The present results from this analysis have been very encouraging when compared with the unsteady fuselage pressures. The 4/rev. pulses on the fuselage due to blade passage effects have been predicted on both the top and sides of the fuselage. The phase effects between the pressure signatures on the left and right hand sides of the fuselage have also been predicted. In addition, it has been found that the unsteady contributions to the fuselage pressures from the changing source strengths on the fuselage are important, and generally cannot be neglected without sacrificing predictive accuracy.

The unsteady pressure signatures on the fuselage in regions of near or very close wake interaction (but not impingement) can be well predicted if both the basic wake geometry is accurately predicted and local wake distortion due to the fuselage is accounted for. Current predictions are deficient in regions of direct wake impingement. In these cases, viscous interactions play a strong role in the process and appear to be beyond the capabilities of a simple model.

References

1. Leishman, J.G., Nai-pei Bi, Samak, D.K., Green, M. "**Aerodynamic Interactions Between a Rotor and a Fuselage in Forward Flight**," Proceedings of the *45th Annual Forum of the American Helicopter Society*, Boston, MA, May 1989.

2. Leishman, J.G., Nai-pei, Bi, "**Measurements of a Rotor Flowfield and its Effects on a Fuselage in Forward Flight**," Under peer review. (Available from the authors).

3. Light, J.S., Frerkin, A., Norman, T., "**Sudies of the Rotor Wake Geometry in Forward Flight using Wide-Field Shadowgraphy**", To be presented at the 46th Annual Forum of the *American Helicopter Society*, Washington D.C. May 1990.

4. Nai-pei Bi, Leishman, J.G., "**Experimental Study of Aerodynamic Interactions between a Rotor and a Fuselage**," Presented at the *5th AIAA Applied Aerodynamics Conference*, Seattle, Washington, August 1989.

5. Crouse, G.L., Leishman, J.G., Nai-pei Bi, "**Theoretical and Experimental Study of Unsteady Rotor/Body Aerodynamic Interactions**". To be presented at the 46th Annual Forum of the *American Helicopter Society*, Washington D.C. May 1990.

NEW VORTEX/SURFACE INTERACTION METHODS FOR THE PREDICTION OF WAKE-INDUCED AIRFRAME LOADS

T.R. Quackenbush
Continuum Dynamics, Inc
Princeton, NJ

D.B. Bliss
Duke University
Durham, NC

G. Lam
Continuum Dynamics, Inc.

A. Katz
Duke University

ABSTRACT

New analytical and computational techniques have been developed at Continuum Dynamics, Inc. and Duke University for the analysis of the interaction of the rotor wake and fixed surfaces. Previous work (Ref. 1) focused on the prediction of flow fields downstream of helicopter main rotors using an advanced free wake analysis, as well as the demonstration of new techniques for the study of vortex/surface interactions in the context of two-dimensional model problems. The current presentation will discuss the status of follow-on work on these topics, including correlation studies on rotor/body flow fields, generalization of previous work to the analysis of unsteady loads generated by three dimensional wake/airframe interactions, and fundamental studies of close vortex dynamics in close proximity to surfaces to support numerical modeling of filament pinch-off.

Recent work (Refs. 2-3) has led to the development of a full-span free wake model of the rotor; this model features a novel discretization of the vortex sheet featuring an array of nonintersecting, constant-strength filaments composed of curved vortex elements. Previous efforts (Refs. 1 and 4) have demonstrated the success of this type of model in predicting both time-averaged flow field data and measured low-frequency response of helicopters to control inputs. However, while the analysis of wake-induced flow fields is critical to the success of any treatment of rotor/airframe interaction, it is only one aspect of the rotor/body interaction problem. Correct simulation of fuselage and empennage effects on the main rotor is also required, as is accurate resolution of loads due to close vortex/surface interaction.

As to the first of these issues, part of the presentation will describe the coupling of a surface panel analysis suitable for the simulation of fuselage-type bodies to the advanced main rotor wake model just described. The results of preliminary validation

runs showing comparisons to the flow-field data of Reference 5 will be included. Also, attention will be given to the discussion of the importance of the nonlinear features of wake/airframe interactions and to the necessity of accurately treating wake deformation near the fuselage.

The presentation will also discuss the coupling the tools developed previously to new approaches to close vortex/surface interaction. In Reference 1, the preliminary steps were taken in the development of new methods that could predict the physically correct free motion of vortex filaments in close proximity to bodies and aerodynamic surfaces. A central feature of this work was the use of local analytical solutions matched into the overall flow field, one application of the general technique of Analytical/Numerical Matching (ANM). Traditional panel method analyses require extremely high surface panelling density to achieve accurate treatment of such close interactions. This circumstance leads to inefficient modeling of bodies and surfaces, since panels must be inserted that are smaller than the vortex core size, which is much smaller than is needed for any other reason.

The close interaction model discussed in Reference 1 involves a preliminary computation with an artificially large ("fat") core on the vortex filaments encountering a panelled body. The flow may be adequately resolved using relatively sparse panelling, but represents a physically incorrect result. This solution can be adjusted by adding in correction terms in the form of an opposite-sign fat core solution and a local solution using the correct sign of vorticity and core size. The result is a composite solution for the velocity field in close proximity to surfaces that produces very accurate results, as seen in Reference 1.

The presentation will discuss the extension of these methods to predict not only the velocity field but the surface pressures generated in realistic, three-dimensional vortex encounters with solid bodies including rotor/body calculations. In addition, the savings in computation time achieved with the relatively sparse panelling that can now be used due to the inclusion of the highly accurate local solution will be discussed, long with conclusions on the sensitivity of the calculations to the choices of panel size and fat core size.

Finally, work is also underway on studies of the fundamental aspects of vortex/surface interaction. An asymptotic solution is being developed for close

proximity interactions of curved vortex filaments with smooth surfaces. This solution models the final stages of the interaction just prior to the onset of strong viscous effects. The surface is modeled by an image filament. In the final stages of the interaction, the filament motion is dominated by nearfield effects. The filament can be characterized by the minimum distance from the surface, the circulation, the radius of curvature, the core size, and the orientation angle. The velocity that determines the convective motion of the arc is governed by a coupled set of nonlinear equations involving the quantities just described. These equations have been nondimensionalized and solved for a limited range of initial conditions. The results are being used to identify conditions under which the vortex is driven to merge with the surface and to estimate the time for this process to take place. The objective of this work is to provide input to the numerical model of wake/surface interaction to determine if, when, and where filaments should be broken to properly model nearfield interactions. Representative results of the work to date on this topic will be shown in the final presentation.

References

1. Quackenbush, T.R., and Bliss, D.B.: "Free Wake Calculation of Rotor Flow Fields for Interactional Aerodynamics", Proceedings of the 44th Annual Forum of the American Helicopter Society, June 1988.

2. Bliss, D.B., Dadone, L.U., and Wachspress, D.A.: "Rotor Wake Modelling for High Speed Applications", Proceedings of the 43rd Annual Forum of the American Helicopter Society, May 1987.

3. Quackenbush, T.R., Bliss, D.B., and Wachspress, D.A.: "Free Wake Analysis of Rotor Configurations for Reduced Vibratory Airloads", Proceedings of the AHS National Specialists' Meeting on Rotorcraft Dynamics, Nov. 1989.

4. Curtiss, H.C., and Quackenbush, T.R.: "Rotor Wake Effects on Helicopter Handling Qualities", Proceedings of the the Fifteenth European Rotorcraft Forum, Amsterdam, the Netherlands, Sept. 1989.

5. Hoad, D.R., Althoff, S.L., and Elliott, J.W.:"Rotor Inflow Variability in Forward Flight", Proceedings of the 44th Annual Forum of the American Helicopter Society, June 1988.

THE INTERACTION OF A ROTOR WAKE AND AN AIRFRAME WITH AND WITHOUT FLOW SEPARATION

J-M. Kim, O.A. Schreiber, S.G.Liou, N.M. Komerath, H.M.McMahon
School of Aerospace Engineering
Georgia Institute of Technology
Atlanta, Georgia 30332

ABSTRACT

The strategy adopted at Georgia Tech has been to conduct a systematic series of studies, using experimental and computational methods, to understand the aerodynamics of a geometrically simple rotor/airframe configuration in low-speed forward flight. The chosen configurations have been useful in highlighting the dominant interaction phenomena, and are amenable to detailed examination and analytical modeling. This abstract discusses four distinct issues: a) the experimental data acquired using an initial configuration chosen to avoid large-scale flow separation effects, b) two computational approaches used, and their status in calculating the aerodynamics of this configuration c) experiments performed to study vortex-surface interaction phenomena in detail, and d) the current experimental program on studying the effects of massive flow separation on the interaction problem.

Basic Experimental Configuration

Figure 1 shows the basic rotor/airframe configuration, installed in the John J. Harper 7' x 9' wind tunnel. The 2-bladed rotor, which is a stiff single piece with fixed collective pitch, is suspended above a sting-mounted hemisphere-cylinder. Two different rotors have been used: one with constant chord, and the other with a 3:1 taper starting at mid-radius. This yields two test cases with significantly different wake and vortex characteristics. There is no other instrumentation on the rotors except for shaft accelerometers (for safety) and a shaft encoder which provides a 1-per-rev reference azimuth pulse. When necessary, the rotor can be mounted on a frame connected around the test section to the external tunnel balance for accurate force measurements, without modifying the flow field in any way. Rotor thrust measurement accuracy is ± 0.1 lb.The airframe is instrumented with 94 static pressure taps and 18 microphone ports; a simple provision for traversing only the front part of the airframe (with a telescoping arrangement) allows collection of microphone data at continuously variable spatial locations. Axial symmetry permits use of a single line of pressure taps to collect static pressure data at any waterline around the airframe. A laser Doppler velocimeter permits measurement of the phase-resolved velocity variation above and below the rotor tip path plane, in the rotor wake, and on the side of the airframe that is optically accessible. The laser also permits the use of strobed, dynamic flow visualization to record vortex behavior. The airframe can be fixed at varying heights and axial positions, or removed entirely, in order to vary the intensity of interaction effects. To-date, all data have been acquired with the airframe at zero angle of attack with respect to the tunnel freestream.

Table 1 shows the different test cases run; for each case, the static pressure distribution has been acquired, and some distributions of unsteady surface pressure have been obtained. Table 2 shows the test cases where data have been acquired with the laser velocimeter. Three kinds of data are involved:a) the downward and vertical components of velocity at points at a fixed distance of 0.5" above and below (inflow and wake) the rotor disc, b) the same components, measured along lines parallel to the airframe axis, at a few different waterlines of the airframe c) more detailed data, acquired during vortex-surface interaction near the airframe surface. Laser sheet visualization studies have documented the dynamics of the vortex system of the

configuration at a variety of test conditions. The surface pressure data have been published as data reports, in addition to journal articles on the measurements, and are also available in electronic form. The velocity measurements have been published, and the data have been compiled into a data report, which is available in a preliminary version, and is currently being modified for easier user access to the computer data files. The flow visualization data are as yet available only from published papers and one videotape of excerpts.

In addition, some restricted kinds of measurements have been made to investigate particular phenomena. These include stagnation pressure variations, surface tuft studies, high-resolution microphone measurements, and pressure spectra.

Some major conclusions from the experiments are:
1. This is a configuration where the interaction effects are strong and clearly identified.
2. The periodic excursions in surface pressure far exceed the time-averaged changes.
3. The primary sources of airframe surface pressure fluctuations are the motion of bound circulation of the rotor blades over the surface, the impingement of the tip vortex on the surface, and the impingement of the vortex sheet on the surface, in that order of magnitude for close rotor / airframe spacing.
4. The dominant effect of the airframe on the rotor flow field is to shift the locations and trajectories of the vortices near the rotor disc.
5. No flow separation has been detected around the cylindrical airframe, even with the impingement of the rotor wake. The only exception is the localized flow reversal during vortex impingement.
6. The observed phenomena are all periodic, with random deviations from periodicity being extremely small.

Computational Studies

The first phase of the computational effort was to develop an "interim" code which would synthesize existing methods for computing rotor aerodynamics and airframe aerodynamics, in order to explain the dominant observed features of the interaction. The result of this effort is the series of codes which is collectively called "GTRAIC", developed by Dimitris Mavris. These consist of algorithms which use modified versions of the Scully Free Wake code for the rotor and of the AMI VSAERO code for the airframe, and an interaction module developed by Mavris, in an iterative sequence. The Free Wake code and VSAERO yield excellent results for their particular problems of specialty, namely, the free wake geometry of an isolated rotor at a given azimuthal location and the static pressure distribution of an isolated airframe subject to an instantaneous distribution of onset flow. The interaction module involves the addition of unsteady potential terms, or, alternately, the addition of models for stagnation pressure rise. In addition, the detailed effect of the passage of the bound circulation distribution of the rotor blades must be specifically modeled, since the Free Wake code uses only a lifting line. The analysis is still subject to the restriction that absolute periodicity is assumed, and one proceeds in specified steps of "frozen" rotor azimuth, with the unsteady effects of rotor motion added on.

GTRAIC has successfully and quite accurately modeled both the periodic pressure variation, and the periodic velocity variation, along the top surface of the airframe under rotor wake interaction. The time-averaged values, computed from these, also match experimental data quite accurately. Around the sides of the airframe, problems are encountered, which have been traced to difficulties in modeling the precise mechanism of vortex-surface interaction. The computed results are consistent with expectations based on potential flow theory; the experimental results are not.

An entirely different approach has been adopted by Olivier Schreiber. He has developed an unsteady Lagrangian vortex-point model for the rotor wake, coupled with a boundary element formulation for the airframe. The present version of the resulting code, which is in a vectorized form suitable for parallel computations, runs on a CRAY-YMP supercomputer, and is being installed on a massively parallel machine. A videotape of intermediate results is included in the presentation. At the present stage, the general features of blade passage are clearly seen on the airframe surface. The detailed vortex-surface interaction remains to be modeled with finer temporal resolution.

Vortex-Surface Interaction Phenomena

Within the framework of the basic configuration, a series of detailed experiments was performed in 1988-89 to study the phenomena occurring during the short time interval when the vortex structures actually interact with the airframe surface. These studies have been described in a series of three publications. The measurements included velocity, surface pressure and vortex dynamics during the tip vortex-surface interaction. The sequence of events on the top surface of the cylindrical airframe, where the cross-section of the vortex can be considered to undergo a quasi-two-dimensional interaction, has been documented. Current efforts are directed towards studying the much more complex three-dimensional phenomena along the sides of the airframe, where the interaction geometry is oblique. The different interaction geometries are illustrated in Fig. 2.

Conclusions to-date from the vortex-surface interaction studies:
1. The deflection of the vortex system near the airframe is qualitatively consistent with "image vortex" models, but quantitatively far more complex
2. Upon impingement, the vortex breaks into at least two distinct features, which then go down the sides of the airframe, and separate streamwise before dissipating. The portions of the vortex filaments that do not impinge on the surface proceed independently down on either side of the airframe.
3. The pressure variation on the surface during vortex interaction is dominated by the stagnation pressure disctribution associated with the tip vortex, as well as by its velocity field.
4. Secondary vortex structures are observed during the vortex interaction. Those that occur ahead of the impingement point are due to flow separation ahead of the stagnation point. Those observed immediately downstream of the impingement region are due to breakup of the tip vortex, which may involve "unrolling" of the rolled-up portions of the vortex sheet. Those observed further downstream are due to vortex sheet effects.

The Massively Separated Flow Case

One important feature of realistic rotor-airframe interactions which is absent by design from the initial test configuration is the presence of large regions of separated flow, such as those behind full-scale rotor masts. The interaction of the periodic, vortical wake with such regions is hypothesized to be a major factor affecting rotor performance and drag. Some indications of such effects are seen in comparisons of Free Wake rotor calculations with experiments. Inflow predictions are seen to differ substantially from experimental data directly downstream of the hub-mast assembly.

It is difficult and expensive to perform fully-viscous 3-d unsteady computations for such configurations. Our approach is to start with a simple model, where the separation line is unambiguously specified. Jai-Moo Kim is currently performing experiments using a backward-facing step geometry obtained by removing the aft portion of the original hemisphere-cylinder airframe, and substituting a cylindrical tube of reduced diameter. Again, axial symmmetry allows examination of the effects all

around the airframe using a single line of pressure taps, and microphone ports. To-date, flow visualization has shown the descent of the vortex system into the separated flow region, where the interaction seems to become more unsteady. The extent of the separated region is seen to vary periodically, as may be expected. The precise nature of the interactions will be studied further by quantitative flow visualization using a new high-power copper vapor laser system, laser velocimetry and pressure measurements.

This experiment, when complete, will provide a basis for developing methods for predicting rotor wake/airframe interactions around much more complex gteometries.

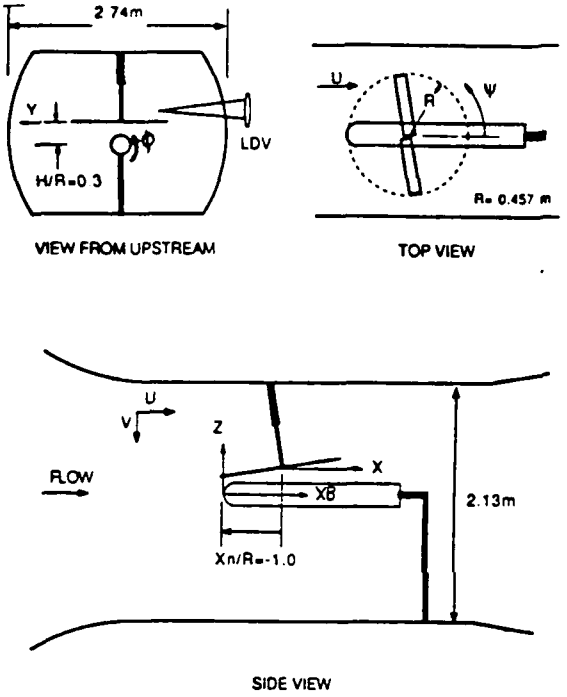

Figure 1: Rotor-airframe configuration installed in the John J. Harper Wind Tunnel.

Table 1: Thrust Coefficient for the two rotors with the airframe present and removed

μ	Rectangular Blade		Tapered Blade	
	Body In	Body Out	Body In	Body Out
0.0	.00633	.00587	.00754	.00720
.075	.00849	.00830	.00966	.00949
.10	.00912	.00890	.0102	.0100
.15	.00970	.00952	.0110	.0109
.20	.0100	.00983	.0115	.0113

Table 2: Summary of Velocity Measurements

TEST CASE		TEST PARAMETERS		
		μ	XN/R	Planform
Rotor Inflow	Body In Body Out	0.1, 0.15	-1.0, -0.6	straight, tapered
Rotor Out-flow	Body In Body Out	0.1, 0.15	-1.0, -0.6	straight
Body Near Field	On Top On Sides Body Out	0.1, 0.15	-1.0, -0.6	straight, tapered
Vortex-Surface Inter--action	Body In	0.1	-1.0	straight

INTERACTION OF DISCRETE VORTICES IN SHEAR FLOWS USING HIGH-ORDER COMPUTATIONAL SCHEMES

by

R.Balasubramanian *

Summary

There are a large number of flow-situations where discrete vortices appear in host flows. The energetics of discrete vortices interacting in shear flows is studied in this work using a high accuracy Spectral collocation (multi-domain algorithm) method. Typical results for interactions in a wall boundary layer of transverse, longitudinal and elliptical ring vortices are presented.

Introduction

Discrete energetic vortices of many sizes and shapes appear in many common flows, e.g., high angle of attack flows, blade tip vortices, the trailing vortices of aircrafts, the convection currents in the ocean and " typical eddys " in turbulent boundary layers. Our understanding of the details of their interactions with one another or with solid boundaries is still very limited. This is highly unfortunate, since, vortical interactions impact on noise, flow separation, dynamic stall and turbulence control. A major source of difficulty that limits our ability to understand these flows containing energetic vortices, is that the interactions are time-dependant and three dimensional, to boot. In many cases, there are highly disparate scales of flow that need to be resolved in order to gain an understanding of these interactions.

We report here on some progress we have made in studies of energetics of vortices imbedded in boundary layer flows, using a newly derived computational algorithm. The essential feature of this algorithm is that it is well-suited for studies of flows with disparate scales, since it employs High Order Spectral Methods and uses a multi-domain patching technique which allows for placement of a highly clustered grid system imbedded in a coarser grid system to resolve the large-small scale features of the flow. Unlike low order finite difference or finite volume methods, spectral algorithms provide for rapidly convergent solutions to the exact. In order to retain the high accuracy of the single-domain Spectral methods in multi-domain patched element method, sufficient care must be taken not to degrade the overall global accuracy by ad-hoc treatment of inter-element boundaries of these patches. In the method that we have adopted here, domains of locally fine and coarse resolutions are patched using a Green's function approach

* Senior Scientist, SPECTREX, Inc.

which provides for C^1 continuity of flow variables. A further feature of the algorithm is that it uses true inflow - outflow conditions, using Chebyshev modes in both streamwise and normal directions (unlike many spectral codes that use streamwise periodicity and a Rayleigh's analogy to relate temporal evolution to spatial evolution).

To gain understanding of vortex interaction in shear flows, we have considered the interaction of an imbedded transverse, longitudinal and an elliptical ring vortex in a host boundary layer. A rational methodology is required for the introduction (i.e. imbedding) and the subsequent evolution of the flow containing these structures. The methodology that we have adopted is as follows:

(a) An initial calculation is conducted for given inflow conditions of velocity at entrance and initial conditions of the flow field in the computational box (normally taken to be that of the inflow field itself). The large time solution of the Navier-Stokes equations provide for the steady-state host boundary layer flow. ($U_0 \{ x, y, z \}$).

(b) The vortex is introduced at a location $[X_0, Y_0, Z_0]$ upstream of the computational box. The convection speed of the vortex is assumed to be that of the host flow at that height. [$U_0 = \{ u (x_1, y_0, z_1), 0, 0 \}$]

(c) Using Biot- Savart law the velocity perturbations at the inflow of the vortex structure is tracked. The composite velocity field at inflow is thus a time-dependant flow condition.

(d) The proper choice of a time step for the calculation of flow field in the computational box using the time-dependant inflow conditions ensures that the vortex entry into the box takes place in a few time steps and that this time is much smaller than the time of transit for the vortex through the computational box. This choice introduces severe perturbations of the order (or higher) of base flow vorticity at the inflow during the entry stages at the inflow for the calculations reported here.

(e) The time dependant flow field in the computational box is obtained at various times by the solution of the Navier-Stokes equation $U \{ x, y, z, t \}$. The difference between the velocity fields constitutes the vortex with its interaction field. Properly storing these data all useful information regarding the vortex and its interaction with the base flow can be viewed.

Results

This approach has been employed to study the flow interactions of transverse , longitudinal and elliptical ring vortices in a base flow of a boundary layer. The base flow considered is a laminar flow of R_x = 5000 -100000. and the vortex Re. No. for these studies ranged from R_v = 65 -2600.

Transverse Vortex

Results of vorticity distributions for a transverse vortex of R_v = 1300 case with the origin of vortex at 0.6δ from the wall are shown in Fig. 1 a,b at some stages of the vortex propagation in the computational cell. It is clear that at latter stages secondary and tertiary structures are formed as a result of the interaction with the shear flow as has been noted by Doligalski et.al. Fig.2 a,b show the vorticity and pressure distribution for the same vortex system. It is to be noted that the vortex system affects the flow only a few core diameters as it enters the box, as can be seen from the Figure. [Isobars remain vertical as should be the case for zero pressure gradient flow (boundary layer) as one moves downstream from the vortex.]

Longitudinal Structures

The interaction of a predominantly streamwise vortex structure in a boundary layer was also studied by us. Such vortex interactions occur commonly when the trailing vortices of aircraft interact with ground plane. The parameter range studied corresponds roughly to the same. Figure 3 a,b,c,d show the midplane vorticity distributions of (Ω_x) at various stages. The interaction of longitudinal structures in flow produces fairly complicated three-dimensional structures.

Elliptical Ring Vortices

Based on the observation by Head and Bandyopadhyay and the full simulation studies of Moin and Kim that turbulent boundary layers consists predominantly of horseshoe structures of various stages of elongation (fat to long and thin noodles at high Re. Nos.) it was decided to study the interaction of these structures in boundary layer by idealising the vortex to an elliptical ring. This structure is introduced at 45° inclination to the flow. Our studies indicate that depending on the nature of rotation, the ring either interacts energetically with the flow being anchored to the wall (even vortex) or lifts away from the wall with little interaction with the base flow (counter vortex). Fig. 4 a,b,c show the stretching of contours as the structure propagates through

the base flow for the even case. The even vortex shows characteristics of turbulent flows based on the rms distribution through the boundary layer of perturbation velocities.

Besides these vortex calculations we have recently been involved in simulation of horseshoe structures in boundary layers by injection of fluid at the wall, thus trying to duplicate the experiment of Acalar and Smith computationaly using the computer algorithm we have developed. Current interests also include full simulation of turbulence using the patched spectral code for higher Re than obtained at Ames by Spalart.

Conclusions

A high order Spectral multi-domain algorithm developed by us has been found to be of use when studying vortex-imbedded flows. Results of the studies of vortex structures in a base flow give some key insights into the role of vorticity in boundary layer eruption, stretching, etc.

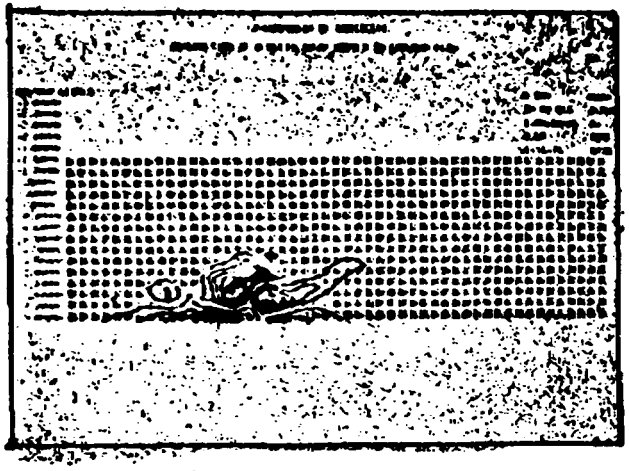

Figure 1(a)

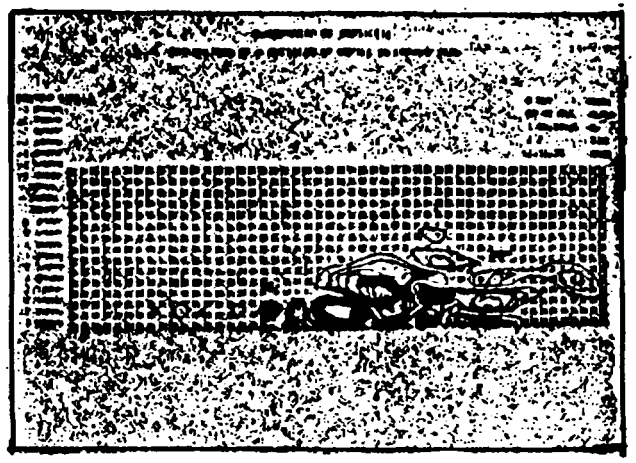

Figure 1(b)

RESULTS OF SPANWISE PERTURBATION VORTICITY DISTRIBUTION FOR A TRANSVERSE VORTEX IMBEDDED IN A BOUNDARY LAYER

R_v = 1300 for this case and the vortex is at 0.6 δ from the wall at birth. Notice that with time the vortex migrates to the wall creating secondary structures in agreement with the work of Doligalski et al.

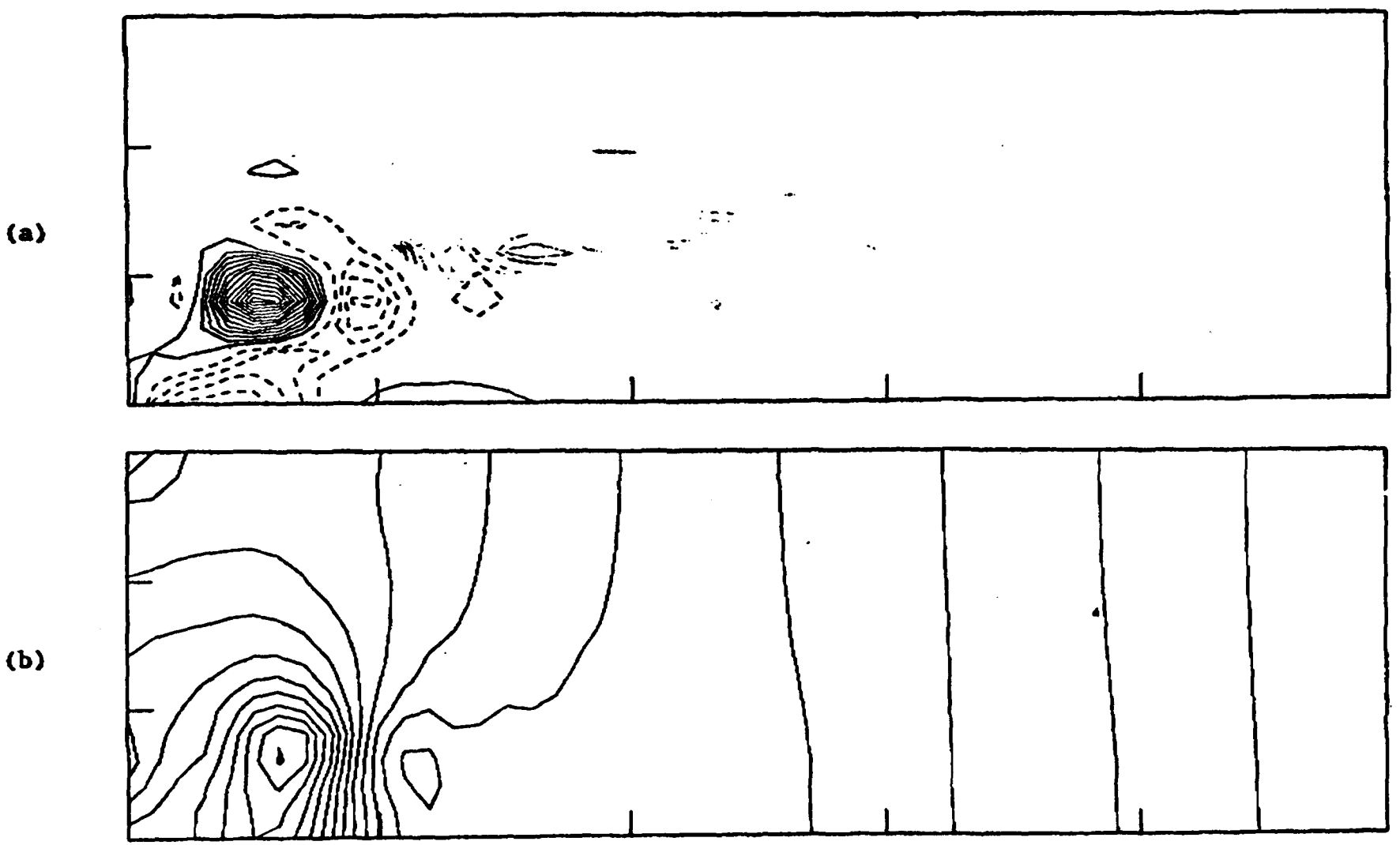

FIGURE 2

TIME= 15; (a) VORTICITY (b) PRESSURE

The transverse vortex system and the perturbation pressure created by it.

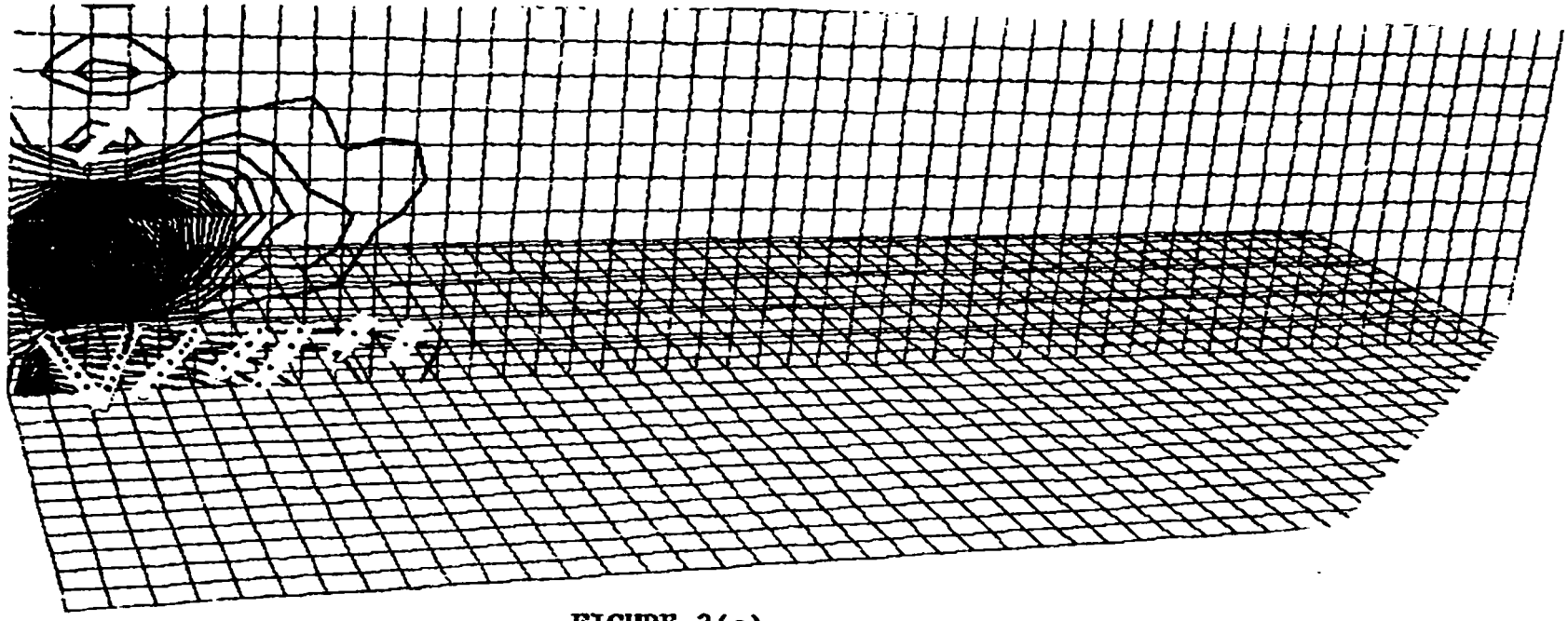

FIGURE 3(a)

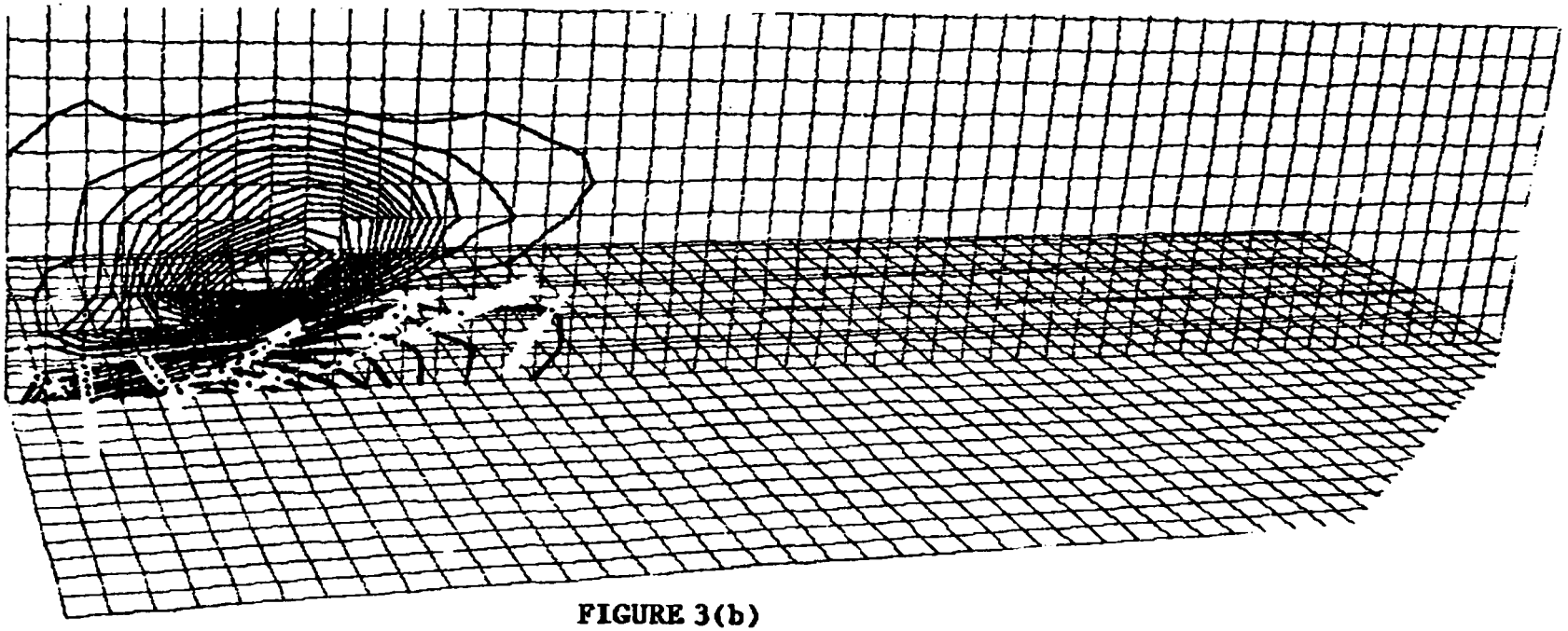

FIGURE 3(b)

Ω_x distribution for logitudinal vortex interaction at midplane at various times (FIGURE 3(a), (b), (c), (d))

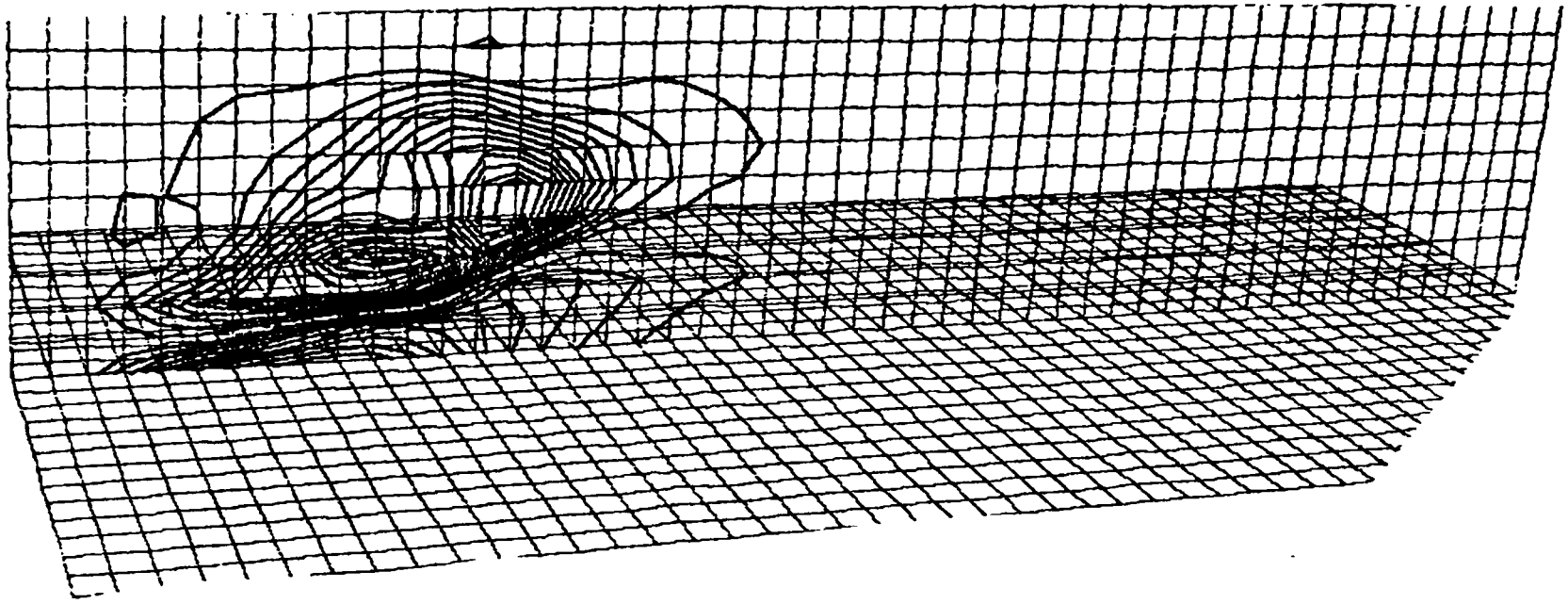

FIGURE 3(c)

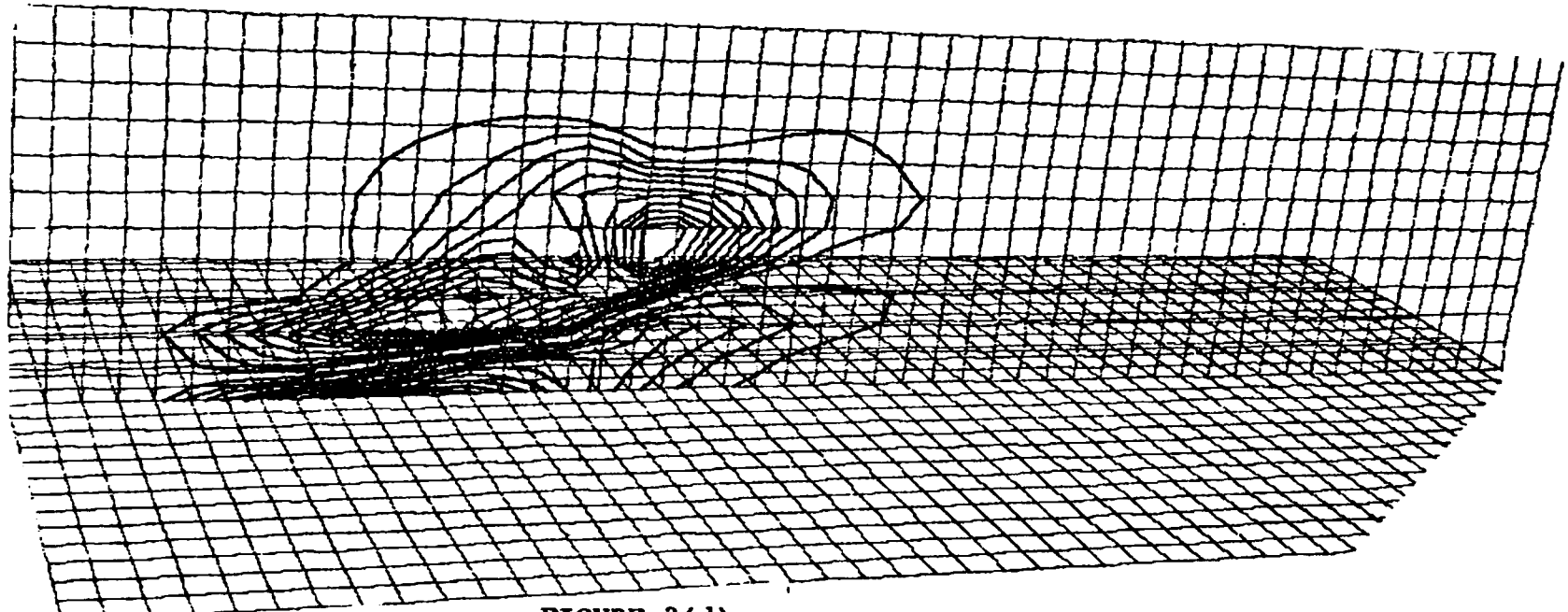

FIGURE 3(d)

Notice the decimation Ω_x as it is convected through the flow. Our studies indicate that longitudinal vorticity is converted to spanwise and normal vorticity by the interaction.

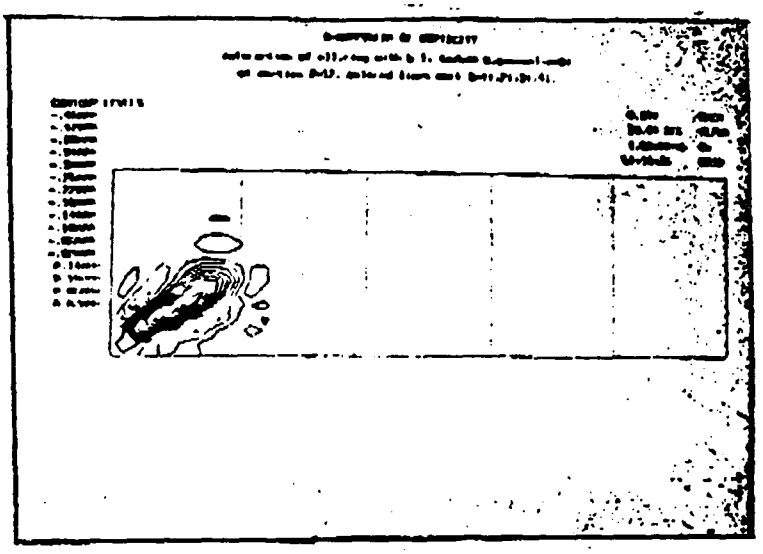

FIGURE 4(a)

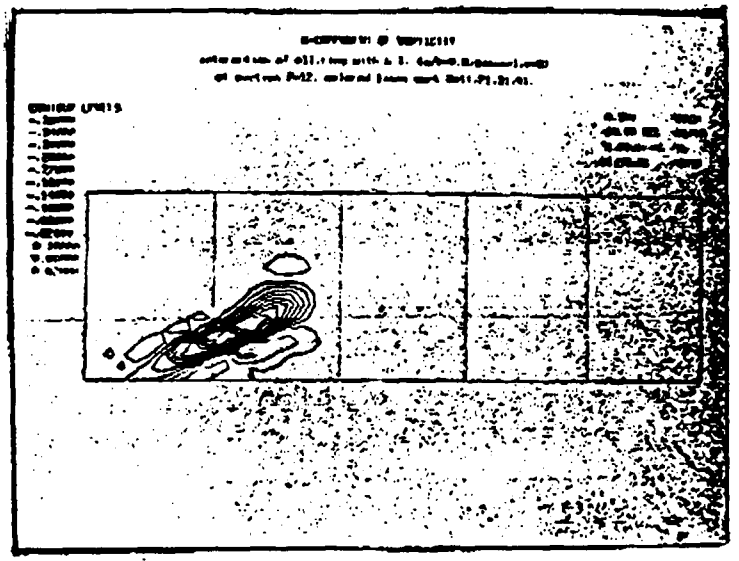

FIGURE 4(b)

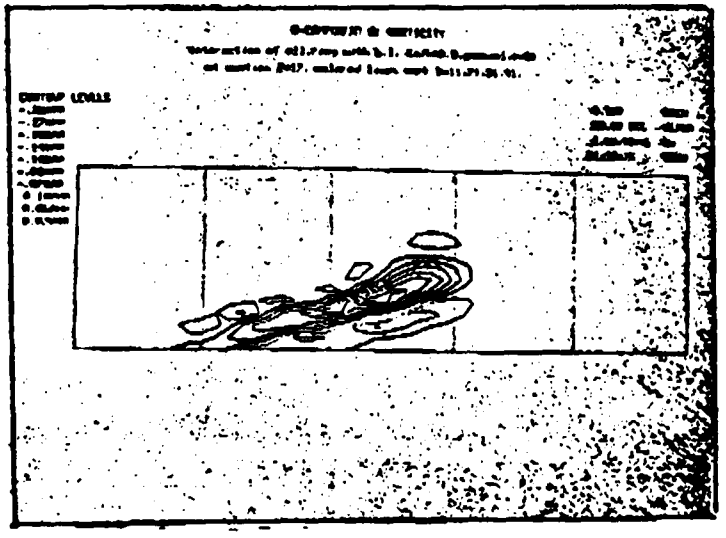

FIGURE 4

Ω_x distribution at a peak plane for an elliptical ring vortex (even) interacting with a boundary layer. Notice the stretching of the vorticity contours as the structure evolves through the flow.

SECOND A.R.O. WORKSHOP ON ROTORCRAFT INTERACTIONAL AERODYNAMICS

HOSTED BY:
THE SCHOOL OF AEROSPACE ENGINEERING
GEORGIA INSTITUTE OF TECHNOLOGY

MARCH 26 - 27, 1990

The Unsteady Interaction of a 3-Dimensional Vortex Filament with a Cylinder

Sponsored by the U.S. Army Research Office

by

H. Affes

and

A. T. Conlisk

DEPARTMENT OF MECHANICAL ENGINEERING
THE OHIO STATE UNIVERSITY
COLUMBUS, OHIO 43210

1. Introduction

The vortex shed by helicopter blades is a complex phenomenon consisting of a highly three dimensional inboard vortex sheet as well as a high-strength tip vortex. Because of increased maneuvering and speed requirements related to the ability to operate in hostile environments, recent work (see discussion by Sheridan and Smith (1980) suggests that much more information about the tip vortex fuselage interaction is required to improve the design of the Army's helicopter fleet. The focus of this presentation is on a simplified model of such a tip-vortex-fuselage interaction and consists of analysis and computation of the motion of an infinitely long vortex filament passing above an infinite circular cylinder. The flow is assumed to be inviscid and irrotational outside the core of the vortex filament.

The motion of three dimensional vortex filaments in free space has been documented by a number of authors and an excellent discussion of the previous work in this area is given by Hon and Walker (1987). For the case where the filament interacts with a body, the amount of work is much more limited; Hon and Walker (1987) consider the motion of a general vortex filament above a plane wall; they are interested in hairpin vortex motion in a turbulent boundary layer. Dhanac (1981) has considered the time evolution of a vortex filament outside a sphere. Of particular interest for the present work is the paper by Liou, Komerath, and McMahon (1989) (see also Brand, McMahon and Komerath (1989)) who measured the pressure and velocity fields for the problem described here; they also produce results for typical vortex trajectories and more will be said about this paper subsequently.

The purpose of the present work is to report on the initial results of the prediction of the motion of a generalized vortex filament above a circular cylinder. Before discussing the results of the present study (section 3), the formulation of the problem is discussed briefly.

2. Formulation

We consider the inviscid flow due to a generalized vortex filament of small cross section; the filament has strength Γ and outside the loop, the flow is assumed to be inviscid and irrotational (figure 1). Then we can define the velocity potential in cylindrical coordinates and this quantity ϕ' satisfies $\nabla^2\phi' = 0$. Let $\phi' = \phi + \phi_v$ where ϕ_v is the velocity potential due to a vortex in free space. Then ϕ satisfies

$$\nabla^2\phi = 0 \qquad \text{with} \qquad \frac{\partial\phi}{\partial r} = -\frac{\partial\phi_v}{\partial r} \quad \text{at} \quad r=1 \tag{1}$$

and ϕ is bounded as $r^2 + z^2 \to \infty$. Here all lengths have been made dimensionless on the cylinder radius a and ϕ has been made dimensionless on $U_\infty a$ where U_∞ is a typical velocity.

To obtain the solution of the boundary value problem (1), we use the Fourier transform in both the z and θ direction (figure 1) and it may easily be shown that the velocity potential due to the presence of the cylinder is given by

$$\phi = -\frac{1}{4\pi^2}\int_{-\infty}^{\infty}\sum_{m=-\infty}^{\infty} e^{im\theta}\left.\frac{\partial\hat{\phi}_v}{\partial r}\right|_{r=1}\frac{K_m(|k|r)}{|k|K_m'(|k|)}e^{ikz}dk \tag{2}$$

where K_m is the modified Bessel function of order m. A mean flow, say ϕ_M may be added to the velocity potential and the total velocity potential ϕ' is thus given by

$$\phi' = \phi + \phi_v + \phi_M \quad . \tag{3}$$

Note that $\partial\phi_v/\partial r|_{r=1}$ is the radial velocity at r=1 due to a vortex filament in free space, which is defined by the Biot-Savart law, and after a significant amount of algebra, the transform of the radial velocity is given by

$$\hat{u}_{rv}|_{r=1} = \int_{-\pi}^{\pi} e^{-im\theta} \int_c \left[ikBK_o(c_1|k|) + A|k|K_1(c_1|k|)\right] e^{-ikz'} ds' d\theta \ . \tag{4}$$

where the c on the integral dnotes integration over the space curve defining the vortex filament ; here A,B, and c_1 are functions of s', angular variable θ, and the filament position and, z'=z'(s). The velocity field is obtained by a straight forward differentiation of equation (3) with subsequent simplification. With an appropriate non-dimensional time scale based on the circulation of the vortex $\Gamma$and the radius of the cylinder, the final form of the total velocity field reduces to

$$\vec{u}'(\vec{x}) = \vec{u}(\vec{x}) + \vec{u}_v(\vec{x}) + \beta\vec{U}_M(\vec{x}) \tag{5}$$

where

$$\beta = 4\pi\frac{U_\infty a}{\Gamma} \ . \tag{6}$$

In this work, the mean velocity field is given by (in cartesian coordinates)

$$\vec{U}_M(\vec{x}) = \left(\frac{\sin 2\theta}{r^2}\right)\vec{i} - \left(1 + \frac{\cos 2\theta}{r^2}\right)\vec{j} + \alpha\vec{k} \tag{7}$$

where $\alpha = W_\infty/U_\infty$ is the ratio of the mean velocity at infinity in the z-direction to the characteristic velocity which is chosen to be the downward mean velocity at infinity.

To convect the vortex filament the curve is parametrized using a parameter s; the typical initial filament profile is given by (in cartesian coordinates)

$$x=f(s) \quad , \quad y=h \quad , \quad z=0 \qquad\qquad -\infty < s < \infty$$

where $f(s)=d_1\sinh(d_2 s)$, d_1 and d_2 are constants. The vortex is discretized using a mesh size Δs and, say $x_j=f(s_j)$ and j=1,.....,n, where $s_1=-1$, $s_n=1$; beyond |s|=1 the filament is assumed to be straight. Each point on the filament is convected in time using Runge-Kutta and all integrals have been evaluated using Simpson's rule. The self induced motion of the filament is computed using the cut-off method described by Hon and Walker (1987).

3. Results

A number of accuracy tests have been performed to insure accuracy of the numerical scheme. Based on these tests L=f(1) was chosen to be 5.0, with Δs=0.05. We should note that a finer grid in s is required if the radius of curvature of the vortex filament becomes smaller as time evolves. To invert the Fourier transform, 40 grid points in k and 40 intervals in θ-direction have been employed. Only 8 modes in m are required for an accurate representation of the azimuthal behavior.

The stagnant flow results are obtained by setting β given by equation 6 to zero and they are shown in figure 2; on this figure the circulation is positive. The initial vortex filament position is represented in cartesian coordinates by x=f(s), y=1.5 and z=0. Note that there are no self-induced velocities associated with this initial configuration because the vortex filament is straight. The only non-zero velocity in this initial configuration is the z-velocity component due to the image of the vortex inside the cylinder. This non-zero velocity is negative if the circulation Γ is positive and it is positive otherwise.It also has a maximum at the center of the vortex and dies out as s tends to infinity. As time evolves, the vortex is increasingly perturbed from its initial position (straight filament) and the self-induced motion becomes more important.

The major influence of the self-induced motion is felt at the center of the vortex which starts to accelarate downward. Thus, as time progresses the vortex evolves into a hairpin-type vortex with the nose moving toward the cylinder in the negative z-direction, and with two legs propagating outward with increasing amplitude as shown in figure 2.

Preliminary mean flow results have also been obtained; we present results here for the parameters $\beta = 3.0$ $\alpha = 2.0$ that appear in equations 6 and 7. Those values correspond approximately to the experimental parameters reported by Liou, Komerath and McMahon (1989).The results are shown in figure 3 for the intial vortex configuration x=f(s), y=2.0 and z=0. These results show consistency with those of the stagnant flow case. However, the downward velocity at the center is relatively smaller than that of the ends of the vortex. The image of the vortex inside the cylinder contributes a negative velocity component in the z-direction (with maximum at the center) which opposes the mean flow one. This results in a smaller total velocity at the center as shown in figure 3. Additional results for the trajectory of the vortex in the vertical cross-section through the cylinder axis are qualitatively similar to those presented in Liou, Komerath and McMahon (1989).

References

Brand, A. G., McMahon, H. M., Komerath, N. M., "Surface Pressure Measurements on a Body Subject to Vortex Wake Interaction," AIAA Journal Vol. 27, No 5, May 1989, pp. 569-574.

Dhanak, M. R., "Interaction Between a Vortex Filament and an Approaching Rigid Sphere,"J. Fluid Mech., Vol. 109, 1981, pp. 129-147.

Hon,L. and Walker, J.D.A., "An Analysis of the Motion and Effects of Hairpin Vortices," Rept FM-11, Dept. of Mechanical Engineering and Mechanics, Lehigh University, 1987.

Liou, S.G., Komerath,N.M and McMahon, H.M., "Measurements of Transient Vortex-Surface Interaction Phenomena," AIAA Paper 89-0833, 1989.

Sheridan, P. F., Smith, R. P., "Interactional Aerodynamics--A New Challenge to Helicopter Technology," Journal of the American Helicopter Society, Vol. 25, No 1, Jan 1980.

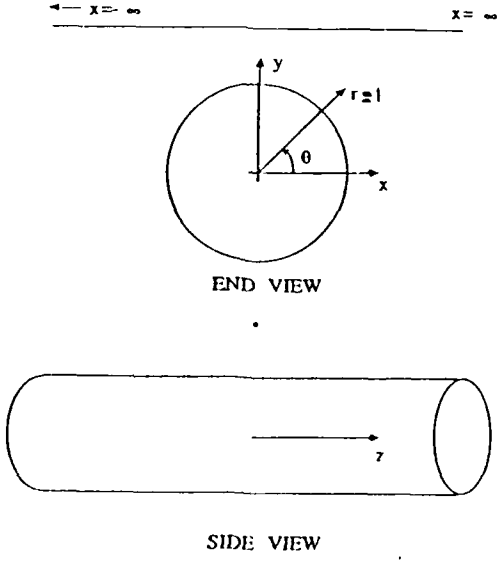

Figure 1. Geometry of the present study. r=1 denotes the cylinder surface.

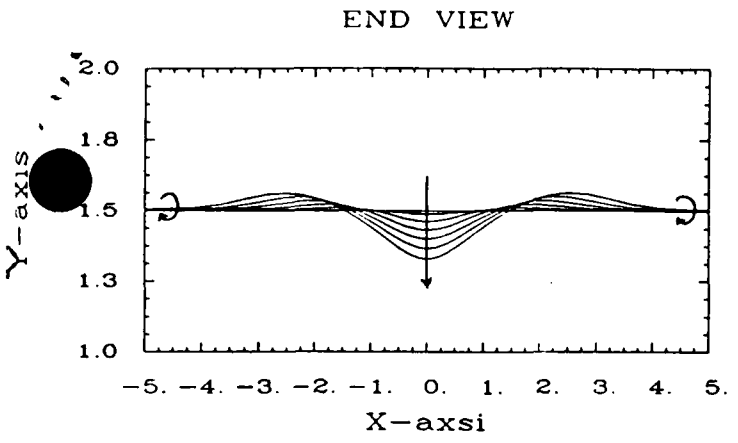

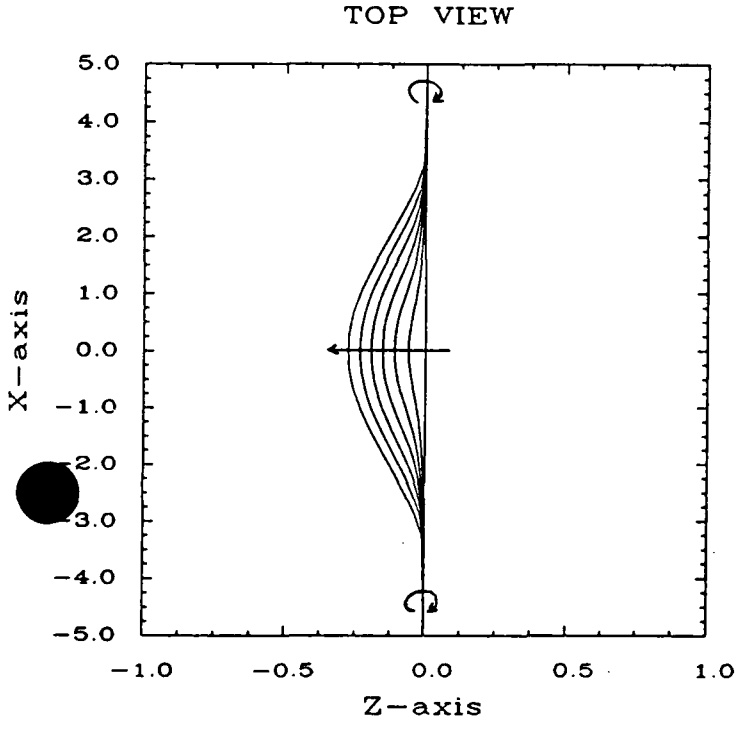

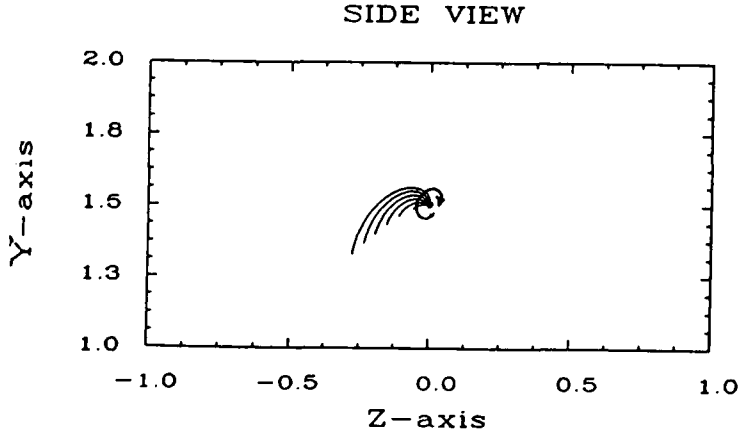

Figure 2. Vortex filament initially placed at y=1.5 z=0, x=f(s) in an otherwise stagnant flow. The lines are plotted every ten time steps (Δt=.01) and the long arrow denotes increasing time. The sense of the circulation is also shown.

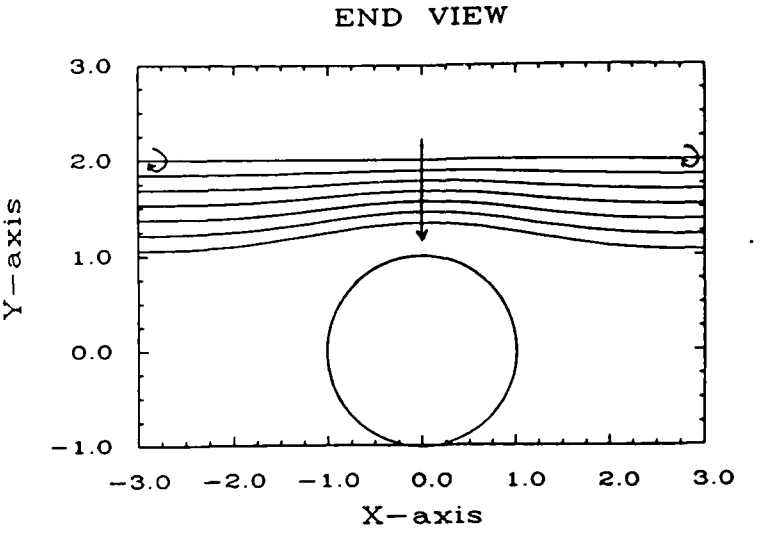

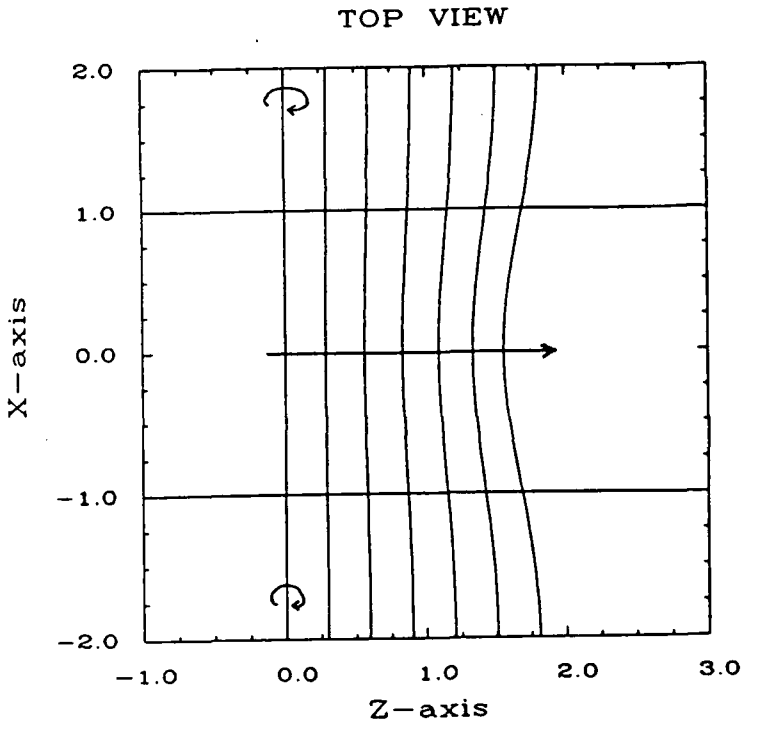

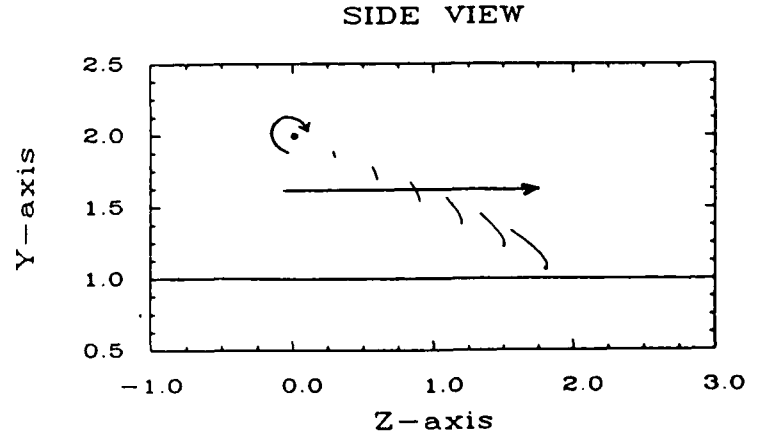

Figure 3. Vortex filament initially placed at y=2. z=0, x=f(s) in a 3-dimensional mean streaming motion. The lines are plotted every five time steps (Δt=.01) and the long arrow denotes increasing time. The sense of the circulation is also shown.